Molecular Studies of Alpha-Scorpion Toxin Interactions with Voltage-gated Sodium Channels

Jinti Wang

A dissertation
submitted in partial fulfillment of the
requirements for the degree of

Doctor of Philosophy

University of Washington

2012

Reading Committee:

Prof. William A. Catterall, Chair
Prof. Neil M. Nathanson
Prof. Ning Zheng

Program Authorized to Offer Degree:

Pharmacology

University of Washington

Abstract

Molecular Studies of Alpha-Scorpion Toxins Interactions with Voltage-gated Sodium Channels

Jinti Wang

Chair of the Supervisory Committee

Professor William A. Catterall

Department of Pharmacology

Voltage-gated sodium channels are responsible for initiation and propagation of the action potential in vertebrate nerve and muscle. They are also the molecular targets for a large number of paralytic neurotoxins.

α-Scorpion toxins, including LqhII (*Leiurus quinquestriatus hebraeus, type II*), bind to the extracellular domain on the sodium channel and inhibit channel fast inactivation. Their binding prolongs sodium channel opening, leading to repetitive firing,

depolarization and conduction block. As a consequence, these toxins can kill organisms by inducing paralysis and cardiac arrhythmia.

Using site-directed mutagenesis, we have identified residues that constitute the functional interaction surfaces of α-scorpion toxin and its receptor site on the voltage-gated sodium channel. Mutants T1560A, F1610A, and E1613A in domain IV had lower affinities for LqhII, and mutant E1613R had ~73-fold lower affinity. Toxin dissociation was accelerated by depolarization and increased by these mutations, whereas association rates at negative membrane potentials were not changed. These results indicate that Thr1560 in the S1-S2 loop, Phe1610 in the S3 segment, and Glu1613 in the S3-S4 loop in domain IV participate in toxin binding. T393A in the SS2-S6 loop in domain I also had lower affinity for LqhII, indicating that this extracellular loop may form a secondary component of the receptor site.

Analysis with the Rosetta-Membrane algorithm resulted in a model of LqhII binding to the voltage sensor in a resting state, in which amino acid residues in an extracellular cleft formed by the S1-S2 and S3-S4 loops in domain IV interact with two faces of the wedge-shaped LqhII molecule. The conserved gating charges in the S4 segment are in an inward position and form ion pairs with negatively charged amino acid residues in the S2 and S3 segments of the voltage sensor. This model defines the structure of the resting state of a voltage sensor of sodium channels and reveals its mode of interaction with a gating modifier toxin.

The bioactive surface of LqhII has recently been shown to be made of a conserved core domain (Phe-15, Arg-18, Trp-38, and Asn-44) and a variable NC domain (Lys-2,

Thr-57, Lys-58). In this work, possible interactions on surfaces of α-scorpion toxin and its receptor site on the voltage-gated sodium channel were tested by thermodynamic mutant cycle analysis. Single mutations at key amino acid residues important for activity on toxin and sodium channel were constructed by mutagenesis. We have identified an intermolecular interaction between extracellular loop of sodium channel and α-scorpion toxins. We demonstrated a specific aromatic-aromatic interaction between amino acid residue Phe1610 and Trp38 of LqhII ($\Sigma\Delta\Delta G$ = 2.45 kcal/mol), a residue that is conserved among many α-scorpion toxins. Toxin dissociation was accelerated by depolarization and increased by mutations at both sites, whereas association rates at negative membrane potentials were not changed for mutation at Phe1610, but slightly increased for mutation at Trp38. These results constrain the possible orientation of α-scorpion toxin with respect to the gating-module of DIV in sodium channel and suggest that upon interaction, the core-domain of LqhII is in close proximity to the sodium channel.

We found that an antianginal and anti-ischemic drug, ranolazine, attenuated sustained Na^+ current induced by α-scorpion toxin, with a 50% inhibitory concentration (IC_{50}) of 102 ± 10.7 μM. It also attenuated the peak Na^+ currents, with an IC_{50} of 334 ± 2.6 μM. The results demonstrate that ranolazine has antagonist effect against α-scorpion toxin. Consistent with this effect on sodium channels, ranolazine reduces the lethal paralytic effects of LqhII in mice.

Table of Contents

List of Figures

Page

Chapter I: Introduction

Functional properties of voltage-gated sodium channels

Sodium channel function

Voltage-gated sodium channels are transmembrane proteins responsible for the rising phase of action potentials in neurons, muscle cells and other excitable cell types. They are rapidly activated when the cell membrane is depolarized, leading to a transient sodium influx, and then inactivated within milliseconds (*1, 2*). The importance of their function is demonstrated by the effects of sodium channel neurotoxins that bind to 6 receptor sites and disrupt its normal behavior (*3, 4*). Due to their high affinity and specificity, these toxins are powerful tools to study the structure and function of sodium channels (*5-8*).

Sodium channel proteins

Voltage-gated sodium channels are heteromeric integral membrane proteins made of a pore-forming α subunit of ~260-kDa and auxiliary β-subunits of 30-40 kDa (*1, 9, 10*). The α subunit is a complex membrane glycoprotein with 24 membrane-spanning segments arranged in four homologous domains. The α subunit is independently functional when expressed in *Xenopus* oocytes or mammalian cells, and contains the ion pore and neurotoxin binding sites 1-6 (*1*), but the kinetics, expression level and voltage dependence of channel gating can be modified by the β subunits (*11-13*). The β subunits are single membrane-spanning glycoproteins (*14, 15*). The β2 subunit is covalently

linked to the α subunit by disulfide bonds, and the β1 and β3 subunits are noncovalently attached. The α subunit consists of four homologous domains, referred to as DI to DIV, that surround a central ion pore, and each domain contains six transmembrane segments (S1-S6) and a membrane-reentrant loop (SS1-SS2) between segments S5 and S6. The S4 segments in each domain serve as the voltage sensors, the S5 and S6 segments and the re-entrant loop between them form the lining of the pore, and the short intracellular loop between domains III and IV form the inactivation gate.

To date, nine sodium channel α subunits, designed $Na_V1.1$-$Na_V1.9$, have been identified and functionally expressed (*16*). They are at least 50% identical in amino acid sequence in the transmembrane and extracellular domains (*16*). $Na_V1.1$, $Na_V1.2$, $Na_V1.3$ and $Na_V1.6$ expressed in brain neurons, and $Na_V1.7$, $Na_V1.8$ and $Na_V1.9$ expressed in dorsal root ganglion cells. The isoform $Na_V1.4$ is expressed primarily in skeletal muscle and $Na_V1.5$ is expressed primarily in cardiac myocytes (*16*).

Sodium channel activation

The ion conductance activity of sodium channels is regulated on the millisecond time scale by intrinsic activation and inactivation gating processes (*17, 18*). In response to depolarization, the S4 segments of sodium channels move outward across the membrane electric field due to electrostatic forces and initiate a conformational change which opens the pore (*18*). The S4 segments in each domain contain repeated motifs of a positively charged amino acid residue followed by two hydrophobic residues and act as voltage sensors (*17-19*). The "sliding helix" model proposed that the gating charges in the S4 segments were paired with negative charges and move outward along a spiral pathway,

exchanging ion pair partners, during activation of the channel (*20-22*). The gating charges are proposed to be stabilized in the transmembrane environment by ion pair formation, and their outward movement is proposed to be catalyzed by sequential, isoenergetic exchange of ion pair partners. This mode of S4 function is consistent with a wide range of structure-function data (*20-23*).

Sodium channel inactivation

Within less than 1 msec after activation, sodium channels inactivate (*17, 18*). In excitable cells, rapid and complete inactivation of sodium channels is very important. Mutations that impair fast inactivation cause inherited periodic paralysis of skeletal muscle, arrhythmias in the heart, and epilepsy in the brain (*24*). Fast inactivation involves the closure of an inactivation gate formed by the cytoplasmic loop connecting domain III and IV of the sodium channel α subunit (*2*). Cutting the loop between domains III and IV by expression of the sodium channel in two pieces greatly slows inactivation (*25*). Mutating a short sequence of a highly conserved hydrophobic motif IFM sequence (Ile1488-Phe1489-Met1490), to Gln slows fast inactivation (*26*). Peptides containing this motif can serve as pore blockers and can restore inactivation to sodium channels having a mutated inactivation gate (*27*). These results support a model in which the IFM motif serves as a tethered pore blocker that binds to a receptor in the intracellular mouth of the pore.

Scanning mutagenesis experiments have revealed multiple amino acid residues that form the inactivation gate receptor site within and near the intracellular mouth of the pore (*28-32*). These amino acid residues are located at the intracellular end of transmembrane

segment IVS6 (*28*) and amino acid residues in intracellular loops IIIS4-S5 (*29*) and IVS4-S5 (*30, 31, 33*). Mutations of residues in these positions destabilize the inactivated state.

Sodium channelopathies

The first sodium channelopathies to be discovered were the familial periodic paralysis syndromes hyperkalemic periodic paralysis (*34, 35*) and paramyotonia congentia (*36, 37*), which are caused by numerous dominant mutations in the skeletal muscle sodium channel. These mutations cause hyperactive sodium channels by impairing the inactivation mechanism or slowing the coupling of activation to inactivation.

Mutations which impair inactivation of cardiac sodium channels lead to a disease of hyperexcitability called inherited long QT syndrome type 3 (*32*). Only a small percent of noninactivating sodium current is sufficient to prolong the action potential. In the electrocardiogram, the interval between the QRS complex and the T wave is prolonged (*32*). Patients with long QT syndrome are at greatly increased risk of life-threatening ventricular arrhythmias. Mutations have been found in the inactivation gate itself and in regions serve as the inactivation gate receptor site and thereby impair channel inactivation (*38, 39*).

Molecular pharmacology of sodium channels

Sodium channels are the molecular targets for a large number of paralytic neurotoxins which bind at six receptor sites (*40*) (Fig. 1). Receptor site 1 is occupied by two different groups of toxins: the water soluble heteocyclic guanidines tetrodotoxin (TTX) and

saxitoxin (STX) and the peptide toxin, μ-contoxins. These toxins block sodium channel conductance by binding to this site. Site 1 is formed by two rings of amino acid residues localized on the N-terminal side of S6 segment in each of four domains of sodium channels (*41, 42*). The first ring is formed by E387, E945, D1426 and D1717 (*41, 42*). The second ring is formed by D384, E942, K1422 and A1714 (*41, 42*). μ-Contoxins share an overlapping but not identical receptor site with TTX/STX (*43*). Additional amino acid residues involved in binding to μ-contoxins have been identified outside of the pore region (*43*).

Receptor site 2 is bound by a family of lipid-soluble toxins including batrachotoxin, veratridine, aconitine, and grayanotoxin, which enhance channel activation (*44*). Photoaffinity labeling and mutagenesis studies implicated transmembrane segments IS6 and IVS6 in the receptor site for batrachotoxin (*4*).

Receptor site 3 is shared by several groups of polypeptide toxins, including α-scorpion toxins and structurally unrelated toxins from sea-anemone and spider venoms (*45-47*). These toxins slow channel fast inactivation. Site-directed mutagenesis has been used to identify the amino acid residues involved in binding to the toxin. Acidic amino acids of the extracellular loops in domains I and IV of $rNa_V1.2a$ were converted to neutral or basic amino acids (*8*). E1613 in the S3-S4 loop in domain IV was identified as a major determinant for both α-scorpion toxin and sea anemone toxin binding (*8*). Subsequent studies indicated that the interaction of α-scorpion toxin and sea-anemone toxin required different molecular determinants on the channel (*8*), even though toxins share overlapping receptor sites.

Receptor site 4 is occupied by another group of scorpion toxins: the β-scorpion toxins, which enhance channel activation (*48-50*). They shift the voltage dependence of channel activation in the hyperpolarizing direction for the brain isoforms, but they have no effect on the voltage dependence of activation of the cardiac isoform $Na_V1.5$ (*51, 52*). Using chimera constructed between brain and cardiac sodium channels has shown that the difference in binding affinity is due to differences in four extracellular loops: S5-SS1 in domain I, S1-S2 in domain II, S3-S4 in domain II and S5-S6 in domain III (*52*).

The lipid-soluble toxins brevetoxin and ciguatoxin isolated from the dinoflagellates *Karenia brevis* and *Gambierdicus toxicus*, respectively, bind to receptor site 5. They cause a hyperpolarized shift of the voltage dependence of channel activation and a block of inactivation (*53*). Photoaffinity labeling experiments have shown that the S6 segment in domain I and S5 segment in domain IV participate in the formation of receptor site 5 (*54, 55*).

δ-conotoxins bind at receptor site 6 and slow sodium channel inactivation. They bind to S4 segment in domain IV, near receptor site 3. Their binding and action is synergistic with α-scorpion toxins (*56*). Both toxins can cause a prolongation of the action potentials.

Scorpion toxins acting on sodium channels

Among the wide range of sodium channel modifiers, those derived from scorpion venoms play an important role. Scorpion venoms are highly complex mixtures of enzymes, peptides, nucleotides, lipids and other unknown substances. Polypeptide neurotoxins are the most abundant group in scorpion venoms and so far the best studied

components. The toxin acting on sodium channel can be divided into two classes, according to their mode of action and binding properties to distinct sites: α- and β-scorpion toxins (*51, 57*). α-scorpion toxins and β-scorpion toxins bind to the neurotoxin receptor site 3 and 4, to inhibit channel fast inactivation and enhance channel activation, respectively (*3*). Toxin binding on the channels can increase channel mean open time, cause inappropriate repetitive firing and disrupt electrical signaling through depolarization. As a consequence, these toxins can kill organisms by inducing paralysis and arrhythmia.

Subtype specificity of α-scorpion toxins

α-Scorpion toxins are divided into three pharmacological groups according to their toxicity in insects and mice and their ability to compete for binding at insect and mammalian sodium channels (*58, 59*): classic α-scorpion toxins, which are highly active in mammalian brain [e.g., AaHII (*androctonus australis*), LqhII (*Leiurus quinquestriatus hebraeus*)]; insect α-scorpion toxins which are highly active in insects (e.g., LqhαIT); and α-like scorpion toxins which are very active in both the mammalian and insect central nervous system (e.g., Lqh-3) (*58, 59*).

The active sites of α-scorpion toxins

The crystal structure of a mammalian-specific toxin from *Androctonus australis* AaHII has been solved at 1.3Å (Fig. 2) (*60, 61*). The three-dimensional structures of other α-scorpion toxins, such as LqhaIT, Lqh3, BmK M1, and AahII, are very similar although they share less than 60% sequence identity. α-scorpion toxins are single chain

polypeptides cross-linked by four disulfide bridges which possess a highly conserved, dense core formed by an α-helix and three strands of β-sheet motifs. These toxins are 61- to 76-residue long. The functional surface is composed of two distinct domains: a conserved "core domain" formed by residues of the loops connecting the secondary structure elements of the molecule core and a variable "NC-domain " formed by a five-residue turn (residues 8-12) and a C-terminal segment (residues 56-64) (Fig. 2) (*62, 63*). Transferring these two distinct domains of insect-selective LqhαIT into mammalian-selective AaHII can result in an insect-selective chimera toxin (*62, 63*). It seems that α-scorpion toxins bind their receptor site on sodium channels by interaction via their two functional domains. Substitutions at each functional domain hamper toxin binding, suggesting that toxin activity requires a cooperative interaction obtained upon binding of the two functional domains to their channels sites.

Insights into the structural basis of the preferential interactions of α-scorpion toxins with insect or mammalian sodium channels were obtained from mutagenesis and crystal structures of toxin mutants (*62-64*). The NC-domain for α-scorpion toxins active on insects protrudes to the solvent (*64*). The NC-domain in anti-mammalian α-scorpion toxins has a flat shape (*64*). The difference in geometry of the NC-domain is due to variations in the backbone conformations. A *cis* peptide bond was observed between amino acid residues 9 and 10 of all α-scorpion toxins active on insects (Lqh3, PDB 1FH3; BmK-M1, PDB 1SN1; BmK-M4, PDB 1SN4), the same bond forms a *trans* conformation in the classic anti-mammalian α-scorpion toxins AaHII and BmK-M8 (*64*). The crystal structure of a toxin chimera, AahIILqhaIT(face), in which the NC-domain of

LqhaIT was constructed on the background of the anti-mammalian AahII toxin, revealed a protruding conformation of the NC-domain (Fig. 3), accompanied by a *cis* conformation of the Asn9–Tyr10 peptide bond (*63*). Since this chimera was highly active on insect sodium channels, but was poorly active on the rat brain Nav1.2a channel, the protruding conformation of the NC-domain seemed critical for the insecticidal potency (*63*).

Structure-function studies only became possible after development of methods for expression and purification of toxins on a large scale. Our collaborators, Dr. M. Gurevitz, Dr. D. Gordon and their coworkers, have established an efficient bacterial expression system to produce large amounts of these polypeptide neurotoxins (*65*). Their methods allow production of these toxins in recombinant form with specific mutations in large quantities to study their function in laboratory.

Mechanism of action of α-scorpion toxins

α-scorpion toxin and sea anemone toxins uncouple activation from inactivation by binding to a receptor site at the extracellular end of the IVS4 segment and preventing its normal gating movement, evidently trapping it in a position that is permissive for activation but not for fast inactivation (*8*). Available data indicates that α-scorpion toxins bind with highest affinity when the channel is closed (*8*). The binding affinity of α-scorpion toxin is decreased by depolarization on sodium channels when S4 voltage sensors are deployed towards the outside (*8*). To alter channel gating, α-scorpion toxins bind to the extracellular S3-S4 loop of domain IV. Toxin binding prevents the conformational change required for fast inactivation. In particular, α-scorpion toxins

block channel fast inactivation by holding the transmembrane segment in domain IV in its inward position. Prolonged depolarization overcomes the effect of toxin binding and drives dissociation as the S4 voltage sensor of domain IV moves outward.

Questions addressed in this research

Based on the background information, research presented in this dissertation aims addressed three central questions:

1. What amino acid residues of sodium channels form the receptor sites for α-scorpion toxin? (Chapter II)

2. What are the specific amino acid interactions of the sodium channel with bound α-scorpion toxins? (Chapter III)

3. Is there an antagonist that can block the α-scorpion toxin function? (Chapter IV)

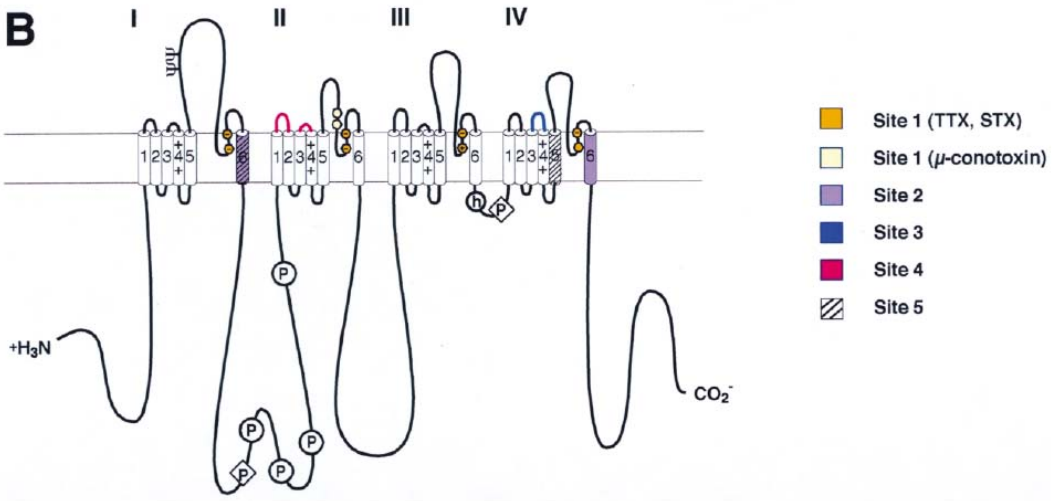

Figure 1 Neurotoxin receptor sites on voltage-gated sodium channels.

Locations of the neurotoxin receptor sites on mammalian sodium channels are illustrated by colors, as indicated in the figure. Adapted from ref (4).

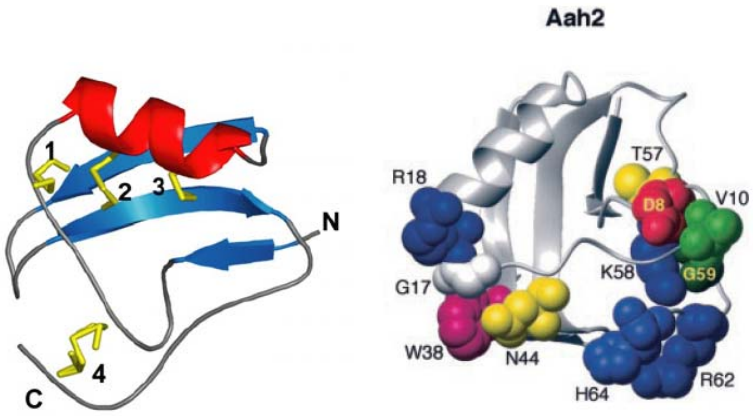

Figure 2 Three-dimensional structure of AaHII (PDB: 1ptx) and its "functional surfaces".

Left panel: Crystal structure of α-scorpion toxin, AaHII. Right panel: The bioactive surface of α-scorpion toxin, AaHII. Adapted from ref (55).

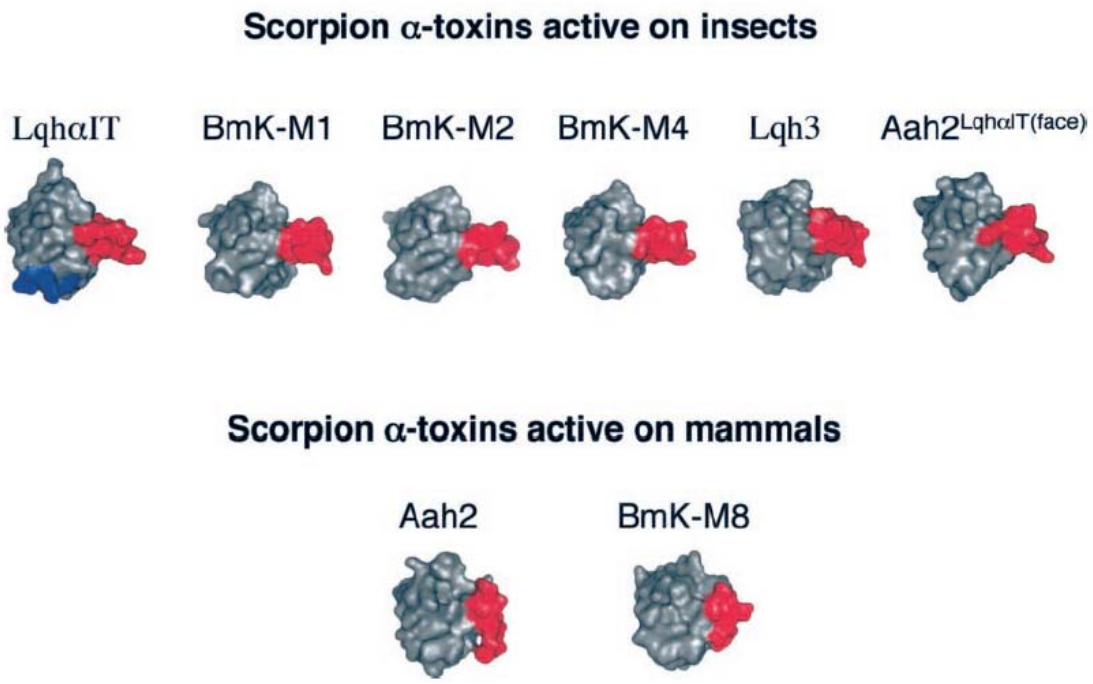

Figure 3 Different conformations of NC-domain in alpha-scorpion toxins active on insects versus mammals.

Adapted from ref (55). There is a protruding conformation of the NC-domain of insect selective α-scorpion toxins and a flat conformation of the NC-domain of mammalian selective α-scorpion toxins.

Chapter II: Mapping the Receptor Site for alpha-Scorpion Toxins on a Sodium Channel Voltage Sensor

Summary

Voltage-gated sodium channels are responsible for initiation and propagation of the action potential in vertebrate nerve and muscle. α-Scorpion toxins, including LqhII (*Leiurus quinquestriatus hebraeus toxin II*), bind to the extracellular surface of resting state of the sodium channel and inhibit fast inactivation. Previous studies with photoaffinity labeling and antibody mapping implicated domains I and IV in toxin binding. Constructs containing mutations of extracellular amino acid residues in domains I and IV of the α subunit of the rat $Na_V1.2$ channel were expressed and tested for receptor function by whole-cell voltage clamp. Most mutant channels had similar toxin binding affinity as wild-type. However, mutants T1560A, F1610A, and E1613A in domain IV had ~5.9-, ~10.7-, and ~3.9-fold lower affinities for LqhII, respectively, and mutant E1613R had ~73-fold lower affinity. Toxin dissociation was accelerated by depolarization for both WT and mutants, and the rates of dissociation were also increased by mutations T1560A, F1610A and E1613A. In contrast, association rates for these three mutant channels at negative membrane potentials were not significantly changed and were not voltage-dependent. These results indicate that Thr1560 in the S1-S2 loop, Phe1610 in the S3 segment, and Glu1613 in the S3-S4 loop in domain IV participate in toxin binding. T393A in the SS2-S6 loop in domain I also showed a ~3.4-fold lower affinity for LqhII, indicating that this extracellular loop may form a secondary component

of the toxin binding site. Analysis with the Rosetta-Membrane algorithm revealed a three-dimensional model of LqhII binding to the voltage sensor in a resting state. In this model, amino acid residues in an extracellular cleft formed by the S1-S2 and S3-S4 loops in domain IV that are important for toxin binding interact with amino acid residues on two faces of the wedge-shaped LqhII molecule that are important for toxin action. The conserved gating charges in the S4 transmembrane segment are in an inward position and form ion pairs with negatively charged amino acid residues in the S2 and S3 segments. This model further defines the structure of the resting state of the voltage sensor in domain IV of sodium channels and reveals its mode of interaction with a gating modifier toxin.

Introduction

Voltage-gated sodium channels are responsible for initiation and propagation of the action potential in vertebrate nerve, muscle, and other excitable cells (*1, 17*). They activate rapidly when the cell membrane is depolarized, leading to rapid sodium influx, and then inactivate within milliseconds (*1, 17*). Several families of neurotoxins bind to six distinct receptor sites on sodium channels and alter their function (*4*). α-Scorpion toxins and β-scorpion toxins bind to neurotoxin receptor sites 3 or 4 and inhibit fast inactivation or enhance activation, respectively (*3*). Their combined effects activate sodium channels at more negative membrane potentials than normal and prolong their opening, leading to repetitive firing, depolarization, and conduction block. As a consequence, these toxins can kill organisms by inducing paralysis and causing cardiac arrhythmia. Due to their high affinity and specificity, these toxins are powerful tools to

study the structure and function of sodium channels (*3, 7, 8, 63, 66*). Identification of the molecular determinants for binding of toxins that modify activation or inactivation will provide important information about structural mechanisms of channel gating and give insight into design of therapeutic agents that could prevent toxin action.

Voltage-gated sodium channels in eukaryotes are heteromeric integral membrane proteins composed of a pore-forming α subunit of 220-260 kDa and auxiliary β-subunits of 30-40 kDa (*1*). The α subunit is functional when expressed by itself in *Xenopus* oocytes or mammalian cells, and contains the ion pore, voltage sensors, and neurotoxin binding sites 1-6 (*1*). It consists of four homologous domains (I to IV) that each contains six transmembrane segments (S1-S6) and a short membrane-penetrating segment (SS1-SS2) between segments S5 and S6. The S5 and S6 segments form the central pore and the SS1-SS2 segments form the ion selectivity filter at its extracellular end. The S1-S4 segments form the voltage sensor. The S4 segment in each domain contains repeated motifs of a positively charged amino acid residue followed by two hydrophobic residues. These positive charges in the S4 segments serve as gating charges and move across the membrane electric field in response to changes in membrane potential, initiating conformational changes that the open and close the pore (*1, 18*). The cytoplasmic linker connecting domains III and IV forms the fast inactivation gate, which folds in and blocks the pore during fast inactivation (*1, 25, 26, 67*).

α-Scorpion toxins are single polypeptides crosslinked by four disulfide bridges, which form a highly conserved, tightly-folded core consisting of an α-helix and three strands of β-sheet (*60*). Neurotoxin receptor site 3 is formed by amino acid residues in the S5-S6

extracellular linker in domain I and the extracellular linker connecting segments S3 and S4 in domain IV, which also contributes to the receptor sites for structurally unrelated toxins from sea anemone and spider venoms (*8, 66, 68-73*). α-Scorpion toxins bind in a state-dependent manner, with high affinity for the resting state (*74*). The voltage sensor trapping model of toxin action posits that binding of α-scorpion toxins prevents the normal outward movement of the IVS4 segment in response to depolarization, thereby trapping it in an inward position and uncoupling activation from fast inactivation (*3*). Prolonged depolarization overcomes the effect of toxin binding and drives dissociation as the IVS4 segment moves outward (*3, 74*).

In order to identify the residues involved in toxin binding and generate a high-resolution molecular model for toxin action, we have constructed mutations in the extracellular loops in domains I and IV. Previous work showed that the conserved acidic amino acid residue E1613 in IVS3-S4 is involved in binding of α-scorpion toxins (*8*), and subsequent studies showed that analogous amino acid residues are important for binding of other toxins to voltage gated K^+ and Ca^{2+} channels (*70*). In this study, we extended molecular mapping of the receptor site for α-scorpion toxins. New amino acid residues in the ISS2-S6 loop, IVS1-S2 loop, and IVS3 segment were identified as components of neurotoxin receptor site 3, and this information was used to generate a molecular model of the toxin-receptor complex in the resting state using the Rosetta Membrane program.

Materials and Methods

LqhII Synthesis.

Production of LqhII, expression in *Escherichia coli*, *in-vitro* folding, and purification of toxin were performed as described previously (*62, 63*).

Site-Directed Mutagenesis.

Mutations were introduced using a PCR-based site-directed mutagenesis strategy as described (*8*). All the WT and mutant channel cDNAs encoding the rat $Na_V1.2$ α subunit were subcloned into the pCDM8 vector.

cDNA Transfection.

tsA-201 cells were transiently transfected with cDNA encoding WT or mutant channels and pEBO-pCD8-leu2, a vector encoding the CD8 receptor, by the calcium phosphate method and plated in a 35-mm dish for electrophysiological analysis. Transfected cells were split 10-20 fold on the day following transfection, and electrophysiological recordings were performed 12-24 hours after transfection. Cells coexpressing sodium channel and CD8 antigen were identified by incubation with polystyrene microspheres coated with anti-CD8 antibody (Invitrogen).

Electrophysiological Recording.

Whole cell voltage clamp experiments were performed using solutions that contained 90 mM CsF, 50 mM CsCl, 10 mM CsEGTA, 10 mM NaF, 2 mM $MgCl_2$, 10 mM Hepes (pH 7.4) in the pipette and 70 mM NaCl, 70 mM N-methyl-D-glucamine, 5 mM CsCl, 1.8 mM $CaCl_2$, 1 mM $MgCl_2$, 10 mM glucose, and 10 mM Hepes (pH 7.4) in the bath (*8*). Toxin was dissolved in the extracellular solution containing 1 mg/mL bovine serum albumin (BSA) to minimize non-specific toxin binding to plasticware. Data collection

was initiated 6 min after breaking the cell membrane to obtain the whole cell voltage clamp configuration.

Data Analysis.

The dose-response for toxin induced removal of inactivation was measured by plotting the ratio of the current at 4 ms after depolarization to 0 mV over the peak current ($I_{4\ ms}$/ I_{peak}) as a function of toxin concentration. K_d was calculated by fitting the dose-response relation to the Hill equation:

$$I_{4\ ms}/\ I_{peak}\ (0\ mV) = 1/\ 1+(K_d/[toxin]^h) \qquad \text{Eq.1}$$

where h is the Hill coefficient, [toxin] is the LqhII concentration, and K_d is the toxin affinity to the sodium channel at -100 mV. All data are reported as mean ± S.E.

Structural Modeling of the LqhII-Na_V1.2 Complex.

Homology and *de novo* modeling of the voltage-sensing domain IV of rat $Na_V1.2$ channel was performed using the Rosetta-Membrane method (*75, 76*). $Na_V1.2$ sequence (residues K1530-G1645) was aligned with Kv1.2 channel sequence (residues A162-H310) using ClustalX software (*77*) (Fig. 10). The $K_V1.2$ channel resting state model (*78*) was used as a template. Five thousand models of the voltage-sensing domain were generated and the lowest scoring model was chosen as the best model. Modeling of α-scorpion toxin was performed using the Rosetta method for modeling of soluble proteins (*79*). α-Scorpion toxin was modeled based on x-ray structure of the scorpion *Androctonus australis Hector* toxin II ((*60*), pdb code: 1PTX) that has ~97% sequence identity with LqhII. 5,000 models of the toxin were generated and the lowest scoring model was

chosen as the best model. Docking simulations of α-scorpion LqhII toxin binding to the $Na_V1.2$ channel domain IV voltage-sensing domain were performed using Rosetta docking method (*80, 81*). Five thousand models were generated and the best model was chosen among 20 lowest scoring models as the model that fit majority of available experimental data on key residues contributing to interaction of the α-scorpion LqhII toxin with the voltage-sensing domain IV of rat $Na_V1.2$ channel (*62*).

Results

Inhibition of Sodium Channel Inactivation by Recombinant α-Scorpion Toxins.

To determine the electrophysiological effects of binding of α-scorpion toxins, wild-type (WT) rat $Na_V1.2$ channels were transiently expressed in the embryonic kidney cell line tsA-201 and analyzed by whole-cell voltage clamp. To determine the K_d, cells were voltage clamped to -100 mV, depolarized to 0 mV to measure the Na current, and tested for modification of fast inactivation by toxin LqhII (*Leiurus quinquestriatus hebraeus,* toxin II), a classic α-toxin that is highly active in mammals (*58*). LqhII was synthesized by recombinant expression in *E. coli*, purified, and renatured. Fig. 4A illustrates superimposed normalized sodium current traces in response to depolarization for WT channels in the absence and presence of 1 nM and 100 nM LqhII. In the absence of toxin, sodium currents activated and inactivated completely within a few ms (Fig. 4A). Addition of 1 nM LqhII slowed the inactivation of a fraction of WT channels, and 100 nM slowed inactivation of most WT channels (Fig. 4A). The fraction of conductance remaining at 4 ms after the peak is proportional to the number of channels modified by

α-scorpion toxin (Fig. 4A). This fraction was measured in the presence of varying concentrations of LqhII and plotted as the ratio $I_{4\ ms}/I_{peak}$ at 0 mV versus toxin concentration (Fig. 4B). These data were fit with a Hill equation (Eq.1) using a fixed Hill coefficient of 1.0. From this analysis, the K_d for LqhII binding was estimated to be 0.47±0.05 nM for WT (n= 3-8), consistent with previous studies of other related scorpion toxins (*8, 74, 82, 83*). The voltage dependence of channel activation was very similar for WT channels in the absence and the presence of LqhII (Table 1).

Molecular Mapping of Amino Acid Residues in the α-Scorpion Toxin Receptor Site in Domain IV of Sodium Channels

Previous work with site-directed antibodies has shown that α-scorpion toxins bind on or near the extracellular loops between transmembrane segments S5 and S6 in domains I and IV (*68, 69*), and more focused site-directed mutagenesis studies showed that the IVS3-S4 loop contains several amino acid residues that have a significant role in toxin binding, with Glu1613 as a primary binding determinant (*8, 69*). We re-evaluated the effects of mutation of Glu1613 in the IVS3-S4 loop using a recombinant α-scorpion toxin, LqhII. Mutant $Na_V1.2$ channels were transiently expressed in tsA-201 cells and analyzed by whole-cell voltage clamp (Fig. 4). The voltage dependence of activation was not significantly changed by either mutation (Table 1), however, the voltage dependence of fast inactivation was shifted to more hyperpolarized potentials by E1613A, but not E1613R (Table 2). The Na^+ currents elicited by depolarization of cells expressing WT, E1613A, or E1613R appeared identical in the absence of toxin. However, a concentration of 1 nM LqhII was less effective in slowing inactivation of E1613A than WT toxin, and

even 10 nM LqhII was less effective in impairing inactivation of E1613R than 1 nM LqhII was on WT (Fig. 4A, C and D). Maximal modification was reached at 100 nM LqhII for both E1613A and E1613R mutants. Averaged results indicated a K_d value at -100 mV of 1.8±0.4 nM for E1613A (n= 3-5), and 34.3±5.7 nM for E1613R (n= 3-4, Fig. 4B, G). Thus, the E1613A mutation reduced the affinity for LqhII ~3.9-fold, and E1613R reduced the affinity for LqhII ~73-fold. These results are consistent with the previous conclusion that E1613 is an important component of the receptor site for α-scorpion toxins.

To develop an accurate molecular model of the toxin receptor site, it is necessary to identify all of the amino acid residues in different extracellular loops that are required for toxin binding. To complete mapping of the receptor site, we analyzed the effects of mutations in the remaining amino acid residues in the IVS1-S2 and IVS3-S4 loops. Hydrophobic amino acids were converted individually to alanine to remove side chain interactions with minimum perturbation of the secondary structure. Charged amino acids were replaced with amides of similar size: glutamine for glutamate, lysine, and arginine, and asparagine for aspartate. Additional residues in the S1, S2, S3 and S4 segments in domain IV were also screened by alanine-scanning mutagenesis. The resulting mutants were tested for binding and action of LqhII by electrophysiology. Mutant F1610A in the IVS3 segment had reduced affinity for LqhII (Fig. 4E). At 1 nM, LqhII was less effective in slowing inactivation of F1610A than WT. The K_d for LqhII was 5.0±1.8 nM for F1610A (n= 3-6, Fig. 4H), ~ a 10.7-fold increase in K_d compared to WT. The voltage dependence of activation was similar for WT and F1610A (Table 1). Phe1610 is located three amino acids residues on the N-terminal side of the E1613 in the IVS3-S4 loop. The

decrease in affinity with alanine mutation at both sites suggests that the side chains of these two amino acids form an essential part of the toxin-binding site.

The results for mutant T1560A in IVS1-S2 also revealed a significant reduction in affinity for LqhII (Fig. 4F) with no significant change in the voltage dependence of channel activation (Table 1). A concentration of 1 nM was less effective in slowing inactivation of this mutant channel than WT, and the concentration-response curve was shifted to higher concentration, with a K_d of 2.8±0.8 nM (n= 4-8, Fig. 4H), ~5.9-fold higher than WT. The decrease in affinity with this individual mutation suggests that the side chain of this amino acid residue may also interact with the toxin directly.

Kinetics of Dissociation of LqhII.

Binding of α-scorpion toxins is reversed by strong depolarizations that activate the voltage sensor (*8, 74*). We investigated the dissociation kinetics of 30 nM or 100 nM LqhII from WT, E1613A, F1610A and T1560A channels using the protocol illustrated in Fig. 5A. Cells expressing each channel type were voltage clamped to -100 mV to allow maximum toxin binding, and then depolarized to +100 mV for an interval varying from 1 to 1024 ms to induce toxin dissociation, hyperpolarized to -100 mV for 20 ms to reverse channel inactivation, and depolarized to 0 mV for measurement of Na^+ current. For WT channels in the presence of 100 nM LqhII, progressively longer durations of depolarization caused progressively faster and more complete Na channel inactivation, which is indicative of LqhII dissociation (Fig. 5A). Dissociation of toxin and loss of toxin action was virtually complete after a 256 ms depolarization to +100 mV (Fig. 5B). The time course of toxin dissociation was determined for the WT channel at three depolarized

potentials, +100 mV, +80 mV and +60 mV, in the presence of 100 nM toxin using the same protocol. The loss of toxin binding with increasing time of depolarization was determined by plotting the fraction of conductance remaining 4 ms after the peak as a function of dissociation time and fitting with a single exponential equation. For WT in the presence of 100 nM LqhII, the dissociation time constant was 94.8±3.3 ms at +100 mV, 135.0±16.9 ms at +80 mV, and 288.3±52.6 ms at +60 mV (n= 3, Fig. 5B). Comparison of these three time constants at different potentials showed that the rate of toxin dissociation was voltage-dependent, with more rapid dissociation during stronger depolarization (Fig. 5C).

The same protocol was then used to measure the dissociation rate for the three mutant channels (Fig. 5C). The WT channel had the slowest dissociation at all membrane potentials. E1613A and F1610A mutations both significantly decreased the time constant by ~4.3- and ~6.7-fold (n= 3), respectively, when measured at +100 mV. The effect was less dramatic for T1560A (n= 3), with ~1.9 fold decrease in time constant at +100 mV. The dissociation time constants were also decreased ~5.8-, ~3.2- and ~1.5-fold, respectively, for E1613A, F1610A and T1560A compared with corresponding values for WT at +80 mV. Similar reduction of the dissociation time constant was also observed at +60 mV. The dissociation time constants for all three mutant channels were voltage-dependent (Fig. 5C), demonstrating that the reduced affinity for these mutants occurs primarily through an increase in the toxin dissociation rate.

The time course of toxin dissociation was also determined for WT and mutant channels in the presence of 30 nM toxin using the same protocol. The dissociation time

constants were 98.3±2.9 ms at +100 mV, 179.6±8.3 ms at +80 mV, and 392.3±20.6 ms at +60 mV for WT (n= 10, Fig. 5D), which again showed strong voltage dependence but little or no concentration dependence indicating that the dissociation step is a unimolecular reaction as expected. The effect of the reduction in time constant of dissociation for all three mutant channels was similar to the results when measured under 100 nM toxin, with E1613A (n= 3) and F1610A (n= 2) giving a dramatic decrease and T1560A (n= 4) giving a modest decrease (Fig. 5D).

Kinetics of Re-association of LqhII.

The rates of toxin association were assessed for WT and mutant channels using a 200-ms prepulse to +100 mV to cause toxin dissociation followed by progressively longer hyperpolarizing pulses to follow the time course of toxin re-binding, and a final test depolarization to 0 mV to assess LqhII action. Fig. 6A shows the stimulus protocol and the superimposed current traces. For WT channels, toxin was dissociated by the depolarizing prepulse as indicated by the rapid inactivation and lack of toxin effect when only 50 ms was allowed for rebinding. Toxin gradually re-bound after longer repolarizations with complete re-association at 12.8 s (Fig. 6B). The time course of toxin re-association was independent of membrane potential at -120 mV, -100 mV and -80 mV in the presence of 100 nM LqhII. Fitting with a single exponential function yielded association time constants of 1.6±0.01 s at -120 mV, 1.2±0.2 s at -100 mV and 1.2±0.3 s at -80 mV for WT channels (n= 3, Fig. 6B and C). In contrast to toxin dissociation, the rate of toxin association was voltage-independent.

The same protocol was used to measure the association rate for three mutant channels, E1613A, F1610A and T1560A, in the presence of 100 nM toxin (Fig. 6C). The rate of toxin association for mutant channels was similar to WT and was voltage-independent. Therefore, these individual mutations did not significantly affect toxin association with the receptor site at hyperpolarized potentials. The time course of toxin association was also determined for WT and mutant channels in the presence of 30 nM toxin using the same protocol. The association time constant was 5.2±0.1 s at -120 mV, 5.4±0.2 s at -100 mV, and 6.8±0.6 s at -80 mV for WT (n= 10, Fig. 6D), which showed ~3.3-, ~4.5-, and ~5.7-fold decrease compared to corresponding values measured at each potentials using 100 nM toxin. Thus, the time constant for association showed strong concentration dependence but little or no voltage dependence, indicating that the association step is a bimolecular reaction with the resting state of the channel. There was no significant change in time constant of association for all three mutant channels measured using 30 nM toxin compared to WT channel (Fig. 6D).

Amino Acid Residues Required for Toxin Binding in Domain I

Antibodies directed against the extracellular SS2-S6 loop of the sodium channel in domain I were effective in immunoprecipitating peptides covalently labeled by a photoreactive α-scorpion toxin and in reducing binding of the α-scorpion toxin LqTxV (*Leiurus quinquestriatus toxin V*) (*68, 69*). Moreover, recent structural studies of $K_V1.2$ channels show that the equivalent of the SS2-S6 loop of those channels interacts with the voltage sensor of the neighboring subunit, implying interaction of the ISS2-S6 loop of sodium channels with the voltage sensor of domain IV (*84*). To identify possible sites of

interaction of LqhII in the ISS2-S6 loop, we tested the amino acid residues from F385 to Y401 by alanine-scanning mutagenesis. Mutant channels were evaluated for toxin action by electrophysiology. Substitution of alanine for most of the residues had insignificant effects, producing changes in K_d of 2-fold or less. However, a ~3.4-fold increase in K_d was observed for mutant T393A (n= 2-5, Fig. 7A and B), resulting in a rightward shift in concentration-response curve. Overall, mutations of T393 and other amino acid residues in the ISS2-S6 loop had less effect on toxin binding, so these residues may form a secondary component of the toxin-binding site.

We also investigated the dissociation kinetics of LqhII from T393A channels. The kinetics of dissociation were measured in the presence of 30 nM or 100 nM toxin using the same protocol illustrated in Fig. 5A. The rate of toxin dissociation was voltage-dependent and generally similar to WT for T393A channels; a slightly increased time constant for T393A was observed at +60 mV for both toxin concentrations (n= 3, Fig. 7C).

The rates of toxin association were assessed for T393A channels using the same protocol as in Fig. 6A in the presence of 30 nM or 100 nM toxin. The association time constant was voltage-independent and showed ~1.2-, ~1.7-, and ~2.2-fold increase compared to corresponding values for WT measured at -120 mV, -100 mV and -80 mV using 100 nM toxin (n= 3, Fig. 7D). The time course of toxin association also showed a similar increase compared to WT when measured under 30 nM toxin at each potential. Thus, this mutation has modest effects on toxin association at hyperpolarized potentials.

Molecular Map of Neurotoxin Receptor Site 3.

The K_d values for all sodium channel mutants that we have studied are summarized in Fig. 8, together with data from our previous work (*8*). Most channels with mutations in domain IV, including those with mutations in the S1 segment, S1-S2 loop, S2 segment, S3 segment, and S4 segment in domain IV, appeared identical to WT with the exception of mutations of three amino acid residues--T1560 in the S1-S2 loop, F1610 near the extracellular end of the S3 segment, and E1613 in S3-S4 loop. These results suggest that the side chains of all three of these amino acids in the extracellular loops in domain IV form a major part of the binding pocket for α-scorpion toxins.

For the SS2-S6 loop in domain I, only T393A gave a substantial ~3.4-fold increase in K_d. All other mutations gave K_d values similar to WT. The structure of Kv1.2 channels reveals that the voltage sensor domain from one subunit interacts closely with the pore domain of the adjacent subunit in a clockwise direction (*84*). These structural results imply that the ISS2-S6 loop is located adjacent to the IVS3-S4 loop in sodium channels. Therefore, it is likely that the amino acid residues in IVS1-S2 and IVS3-S4 form the primary receptor site for α-scorpion toxins, whereas T393 and perhaps other amino acid residues in the ISS2-S6 loop provide a secondary site of interaction.

Structural Model of the α-Scorpion Toxin/$Na_V1.2$ Channel Complex.

We have developed a structural model of the LqhII-$Na_V1.2$ complex using the Rosetta docking method (*80*) and resting state models of the $K_V1.2$ channel (*75, 76, 85*) as a template for the $Na_V1.2$ domain IV voltage sensor (Fig. 9). Our structural model shows that the LqhII toxin has an extensive interface of interaction with the extracellular water-accessible cavity of the $Na_V1.2$ domain IV voltage sensor (Fig. 9). The overall

orientation of the α-scorpion toxin LqhII relative to the voltage sensor in our new model (Fig. 9) is very similar to the orientation of the structurally homologous *Centruroides suffusus suffusus* toxin IV (CssIV) relative to the voltage sensor in domain II (*86*). The wedge-shaped LqhII molecule sits in the cleft between the IVS1-S2 and IVS3-S4 loops and makes intimate contact on two sides of the wedge through interactions with amino acid side chains. The majority of residues in the voltage sensor that have significant effects on LqhII toxin binding are at the interface with the toxin in our model (Fig. 9). LqhII residues Phe15, Trp38, and Asn44 in the core domain of LqhII are buried deeply in the cleft between IVS1-S2 and IVS3-S4 (Fig. 9B, D). Evidently, interactions of the core domain of LqhII with amino acid residues in this cleft in the voltage sensor contribute the majority of the binding energy that drives formation of the toxin-receptor complex. The key amino acid residues in the sodium channel are also positioned to interact with the bound toxin (Fig. 9A, C). Thr1560 in IVS1-S2 interacts with one face of the wedge-shaped toxin while Glu1613 interacts with the other face. In the most stable channel conformation shown in Fig. 9A-D, the side chain of Phe1610 points away from the bound LqhII. However, a slightly different conformation in which the IVS3 helix is unwound beginning at Phe1610 allows its interaction with Phe15 and/or Trp38 in the core domain of LqhII and retains potential interactions of Thr1560 and E1613 with bound LqhII. It is conceivable that toxin binding induces unwinding of the outermost turn of the IVS3 helix and that voltage-dependent outward movement of the S4 segment induces re-winding of the outer end of the S3 segment into helical conformation and consequent dissociation of the bound toxin. Alternatively, it is possible that this unwound conformation of the outer end of S3 is found in the resting state of the channel, even

though it appears to be less stable in Rosetta modeling. New structural details will be required to resolve the precise conformation of the IVS3 segment with LqhII bound.

Discussion

Amino Acid Residues in S1-S2, S3, and S3-S4 Segments in Domain IV Form the Primary Site of Interaction for α-Scorpion Toxins

In previous studies, we found that the acidic amino acid residue Glu1613 in the S3-S4 extracellular loop in domain IV contributes significantly to α-scorpion toxin binding (*8*). In this work, we found two additional nearby mutations that caused substantial reduction in binding affinity for LqhII from ~5.9- to ~10.7-fold: T1560A in IVS1-S2 and F1610A near the extracellular end of IVS3. It is likely that these three amino acid residues form the primary component of the receptor site for α-scorpion toxins. Amino acid residues aligned with Phe1610 and Glu1613 contribute to the ω-agatoxin receptor site in $Ca_V2.1$ channels (*73*) and the hanatoxin and grammotoxin receptor sites in K_V channels (*70, 71*). Thus, these studies reveal a common motif of FXXE that may contribute to the actions of all of these gating modifier toxins (*3*).

Amino Acid Residues in Domain I Form a Secondary Site of Interaction for α-Scorpion Toxins.

Anti-peptide antibody experiments suggested that neurotoxin receptor site 3 is formed by amino acid residues in the segment between amino acids 382 and 400 in the extracellular S5-S6 loop in domain I as well as by the S3-S4 loop in domain IV (*68, 69*). Our experiments identify Thr393 as a primary point of interaction in this segment of the

channel. The structure of $K_V1.2$ channels revealed that the voltage-sensing module from one subunit interacts closely with the pore-forming module of the adjacent subunit in a clockwise direction when the $K_V1.2$ channel structure is viewed from the extracellular side of the membrane (*84*). This organization would place the IS5-S6 segment adjacent to the IVS1-S2 and IVS3-S4 segments in Na_V channels. β-scorpion toxins, which are similar to α-scorpion toxins in structure but enhance activation by binding to the S3-S4 loop on domain II, have been found to interact with amino acid residues in the SS2-S6 loop in the adjacent pore-forming module in domain III as well as with amino acid residues in IIS3-S4 (*87*). Consistent with these previous studies, we found one amino acid residue (Thr393) in the ISS2-S6 loop that contributes significantly to α-scorpion toxin binding, although its contribution was substantially less than the residues in IVS1-S2 and IVS3-S4. These results indicate that α-scorpion toxins have a secondary site of interaction with this segment of domain I. The conformation of LqhII bound to domain IV (Fig. 9) places it in position for the essential amino acid residues in its NC domain to interact with amino acid residues in the S6-SS2 segment of domain I.

Voltage Dependence of α-Scorpion Toxin Binding.

α-Scorpion toxins bind with high affinity to the resting state of sodium channels, and their binding is reversed by depolarizations that activate sodium channels (*74, 88*). By comparing the time constants for toxin dissociation for WT channels at +100 mV, +80 mV and +60 mV, we found that recombinant LqhII dissociates more rapidly at more depolarized potentials, as previously observed for other α-scorpion toxins (*8, 74, 83*). These results indicate that the conformation of the toxin-receptor complex changes

during depolarization from a high affinity conformation in the resting state at negative potentials to a low affinity conformation in the activated state at positive potentials. Evidently, high-affinity toxin binding to the resting state of the voltage sensor opposes the outward movement of the S4 segment in domain IV in response to depolarization, thereby uncoupling channel opening from fast inactivation. However, prolonged depolarization can drive toxin to dissociate from the channel and lead to voltage-dependent dissociation of bound α-scorpion toxin (*74, 88*). Three mutations, (T1560A, F1610A and E1613A) significantly decreased the dissociation time constant ~1.9-, ~6.7- and ~4.3-fold, respectively, when measured at +100 mV, demonstrating that alanine mutations at these three sites reduced the stability of the toxin-channel interaction, making dissociation of the toxin more favorable.

By comparing the time constants for LqhII binding to WT channels at -120 mV, -100 mV and -80 mV, we found that toxin binding to the resting state of sodium channels is voltage-independent. These results indicate that the charged amino acid residues of the toxin do not enter the transmembrane voltage field during binding. Furthermore, the three mutations T1560A, F1610A and E1613A did not change the association time constant significantly at these hyperpolarized potentials in the presence of 30 nM or 100 nM toxin compared to WT. Therefore, the changes in toxin binding affinity to the resting state measured at negative membrane potentials caused by these mutations in domain IV must result from changes in the rate of dissociation. However, the T393A mutation in domain I increased the association time constant from ~1.2- to ~2.1-fold at hyperpolarized potentials, indicating this mutation may affect toxin binding by a different mechanism.

Structure of the Complex of α-Scorpion Toxins with the Resting State of the Voltage Sensor in Domain IV

The structures of voltage-gated ion channels that have been determined to date have had activated voltage sensors (*84, 89-91*), which is expected because the activated state is favored at a membrane potential of 0 mV as in a protein crystal. We have developed a molecular model of the resting state of the voltage sensor of $K_V1.2$ channels using the Rosetta Membrane modeling system (*75, 85*) and the crystal structure of the open state (*90, 91*), and we have used the Rosetta Membrane Docking algorithm (*81*) to construct a model of the α-scorpion toxin-receptor complex. Our structural model (Fig. 9) reveals a close fit of the toxin in the groove between the S1-S2 and S3-S4 extracellular loops of the voltage sensor in domain IV. This docking position of the bound toxin in the voltage sensor closely resembles the position of the β-scorpion toxin CssIV when bound to its receptor site in the voltage sensor of domain II of sodium channels (*86*).

It is noteworthy that our structural model does not reveal interactions of amino acid residues in the N-and C-terminal domains of LqhII with the voltage sensor, even though these amino acid residues are important for toxin binding and action (*58, 63, 92, 93*). We speculate that these amino acid residues may interact with the SS2-S6 loop in domain I, which may form a secondary site for toxin interaction based on our mutagenesis studies. Our current models for the structure of the voltage sensor do not define its spatial relationship with the SS2-S6 extracellular loop in the complete structure. Therefore, a model of this part of the toxin-receptor complex must await determination of the three-dimensional structure of the resting state of a voltage sensor in a complete

voltage-gated ion channel or development of models for the entire four-domain sodium channel structure.

Implications of Voltage Sensor Structure for its Mechanism of Action.

Our model of the resting state of the voltage sensor in domain IV of $Na_V1.2$ channels provides an initial view of the resting state conformation of a sodium channel. As expected from our model of the resting state of $K_V1.2$ channels (*75, 85*), the S4 segment is in a transmembrane orientation in the resting state, and its gating-charge-carrying arginine residues are in an inward position, poised to move outward upon depolarization of the membrane. The R2 gating charge interacts with Asn1567 on the extracellular side of the S2 segment. The R3 side chain is on the intracellular side of the gating pore in position to interact with the conserved negatively charged residues Glu1578 in S2 and Asp1598 in S3. The R4 and R5 gating charges are exposed on the intracellular side of the membrane. These molecular interactions illustrate how the voltage sensor structure stabilizes the gating charges in their inward position in the resting state of the sodium channel and how binding of LqhII traps the voltage sensor in its resting conformation.

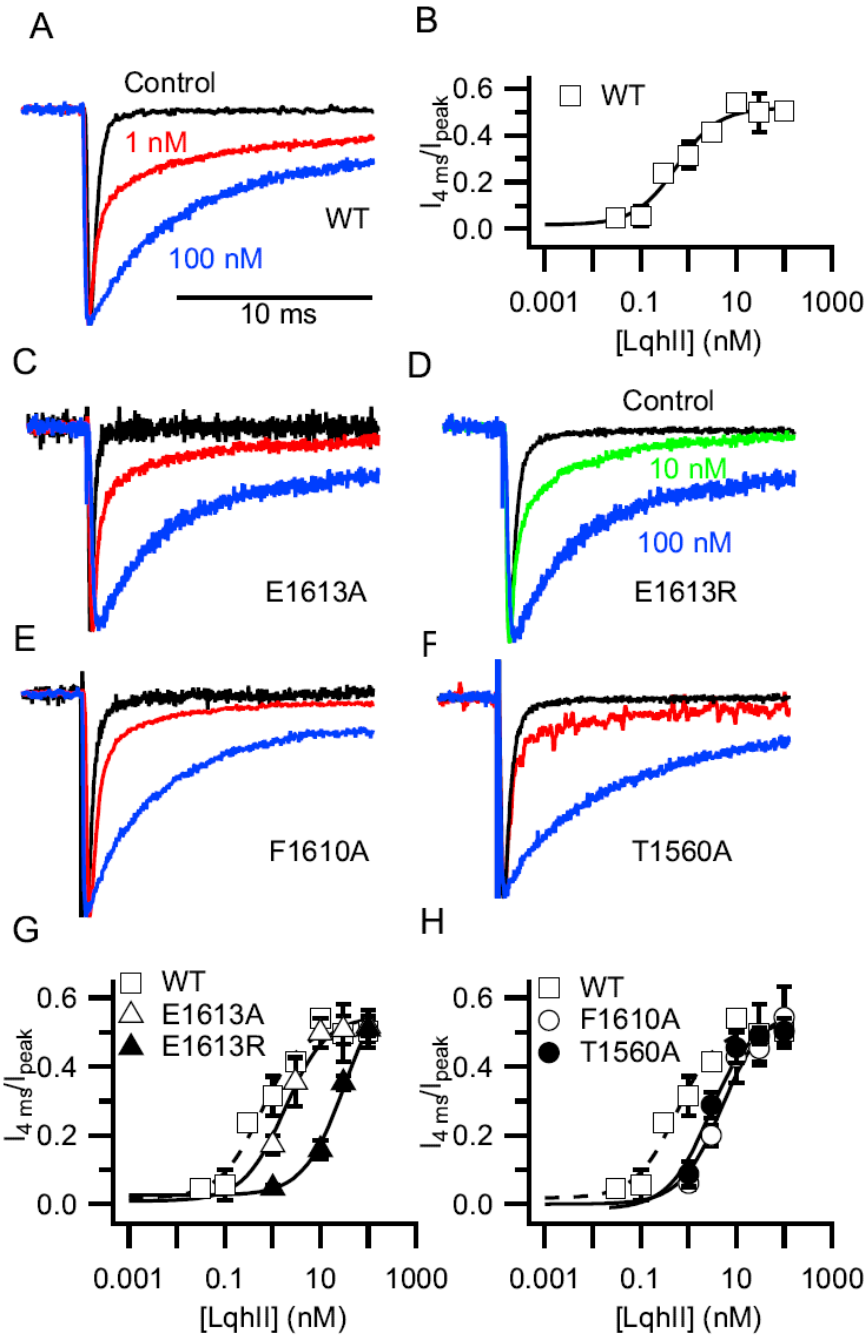
A
Control
1 nM
WT
100 nM
10 ms
B
WT
$I_{4\ ms}/I_{peak}$
0.6
0.4
0.2
0.0
0.001
0.1
10
1000
[LqhII] (nM)
C
E1613A
D
Control
10 nM
100 nM
E1613R
E
F1610A
F
T1560A
G
WT
E1613A
E1613R
$I_{4\ ms}/I_{peak}$
0.6
0.4
0.2
0.0
0.001
0.1
10
1000
[LqhII] (nM)
H
WT
F1610A
T1560A
$I_{4\ ms}/I_{peak}$
0.6
0.4
0.2
0.0
0.001
0.1
10
1000
[LqhII] (nM)

Figure 4 Electrophysiological effect of LqhII on WT and mutant $Na_V1.2a$ channels transiently expressed in tsA-201 cells.

(*A*, *C-F*). Normalized voltage-clamp current traces from tsA-201 cells expressing WT and mutant channels in the absence (Control, black) and in the presence of 1 nM (red), 10 nM (green) or 100 nM LqhII (blue). Cells expressing $Na_V1.2\alpha$ channel were held at -100 mV and Na currents were elicited with a 30 ms step to 0 mV. (*A*)WT. (*C*) E1613A. (*D*) E1613R. (*E*) F1610A. (*F*) T1560A. (*B, G-H*). Concentration-response relations for LqhII block of fast inactivation from cells expressing WT and mutant channels. (*B*) WT (K_d = 0.47±0.05 nM). (*G*) E1613A (K_d = 1.8±0.4 nM) and E1613R (K_d = 34.3±5.7 nM). (*H*) F1610A (K_d = 5.0±1.8 nM) and T1560A (K_d = 2.8±0.8 nM).

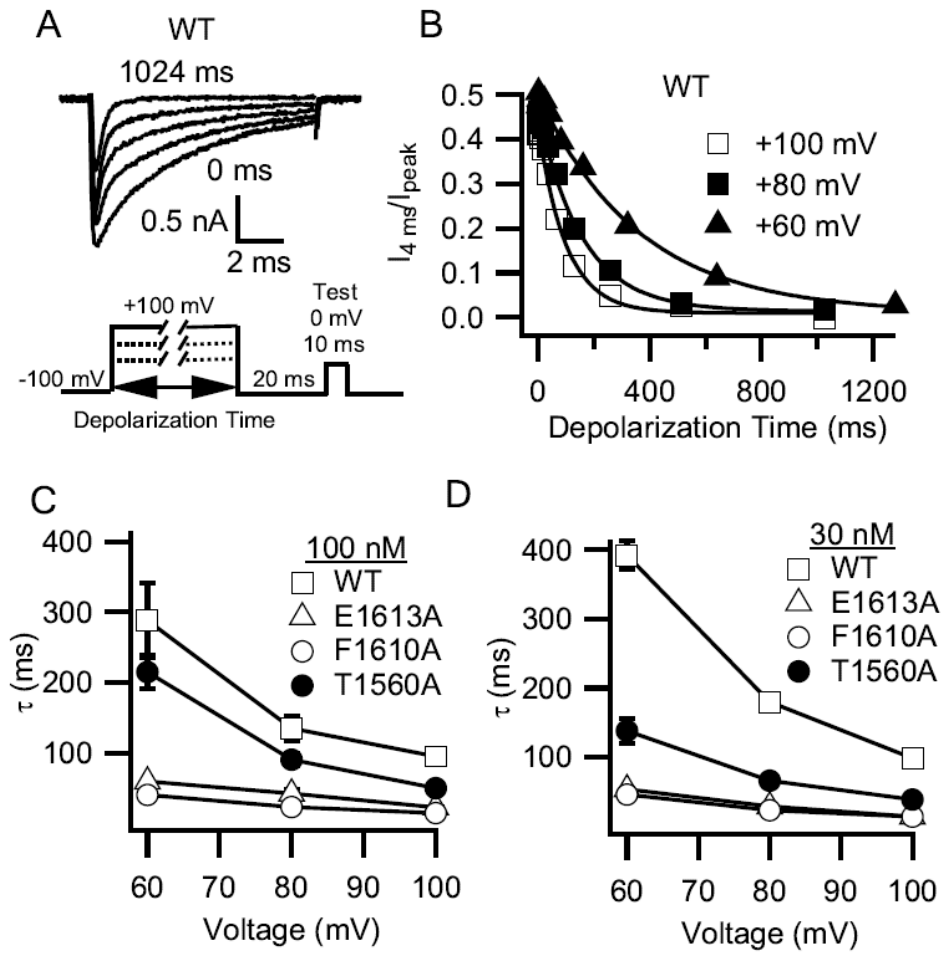

Figure 5 Voltage-dependent dissociation rates of LqhII.

(*A*) Traces demonstrating time-dependent dissociation of LqhII at +100 mV. Cells expressing WT $Na_V1.2$ channels were incubated in 30 nM or 100 nM LqhII for 6 min at a holding potential of -100 mV to allow binding. The rate of toxin dissociation was determined with the illustrated pulse paradigm by stepping to a depolarizing pulse of +100 mV, +80 mV, or +60 mV, for 1 to 1024 ms, returning to -100 mV for 20 ms to allow recovery from fast inactivation and then assessing the effect of the depolarizing pulse with a 10 ms test pulse to 0 mV (test). Traces show the acceleration of inactivation due to toxin dissociation with longer depolarizing pulses for WT channels measured at +100 mV. (*B*) Time course of dissociation of 100 nM LqhII from cells expressing WT channels at +100 mV (τ=94.8±3.3 ms), +80 mV (τ=135.0±16.9 ms) and +60 mV(τ=288.3±52.6 ms). Time constants were determined by fits of mono-exponential functions to the data. (*C* and *D*) Time constants of dissociation as a function of potential for WT, E1613A, F1610A and T1560A channels. (*C* 100 nM LqhII. (*D*) 30 nM LqhII.

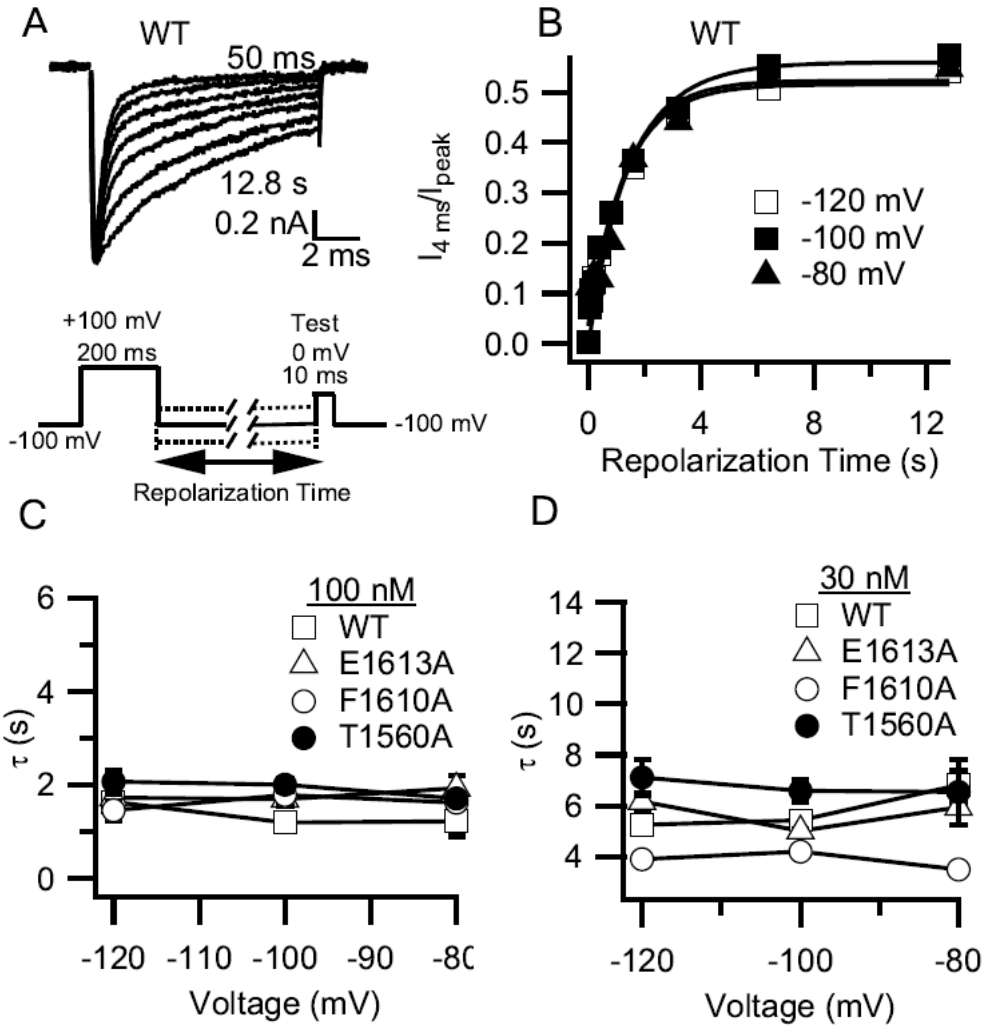

Figure 6 Rates of LqhII association after repolarization.

(*A*) Current traces demonstrating time-dependent reassociation of LqhII at -100 mV. Cells expressing WT channels were incubated in 100 nM LqhII. Toxin was dissociated from the channel using a 200-ms depolarization to +100 mV. The rate of toxin association was measured by hyperpolarizing to -120 mV, -100 mV, or -80 mV for intervals of increasing duration. The effect of repolarization on toxin action was assessed with a 10 ms test pulse to 0 mV (test). Traces show the deceleration of inactivation due to toxin association during longer hyperpolarizations. (*B*) The time course of association of 100 nM LqhII from cells expressing WT channel was determined at -120 mV(τ=1.6±0.01 s), -100 mV(τ=1.2±0.2 s) and -80 mV(τ=1.2±0.3 s). (*C* and *D*) Time constants of association as a function of voltage for WT, E1613A, F1610A and T1560A channels. (*C*) 100 nM LqhII. (*D*) 30 nM LqhII.

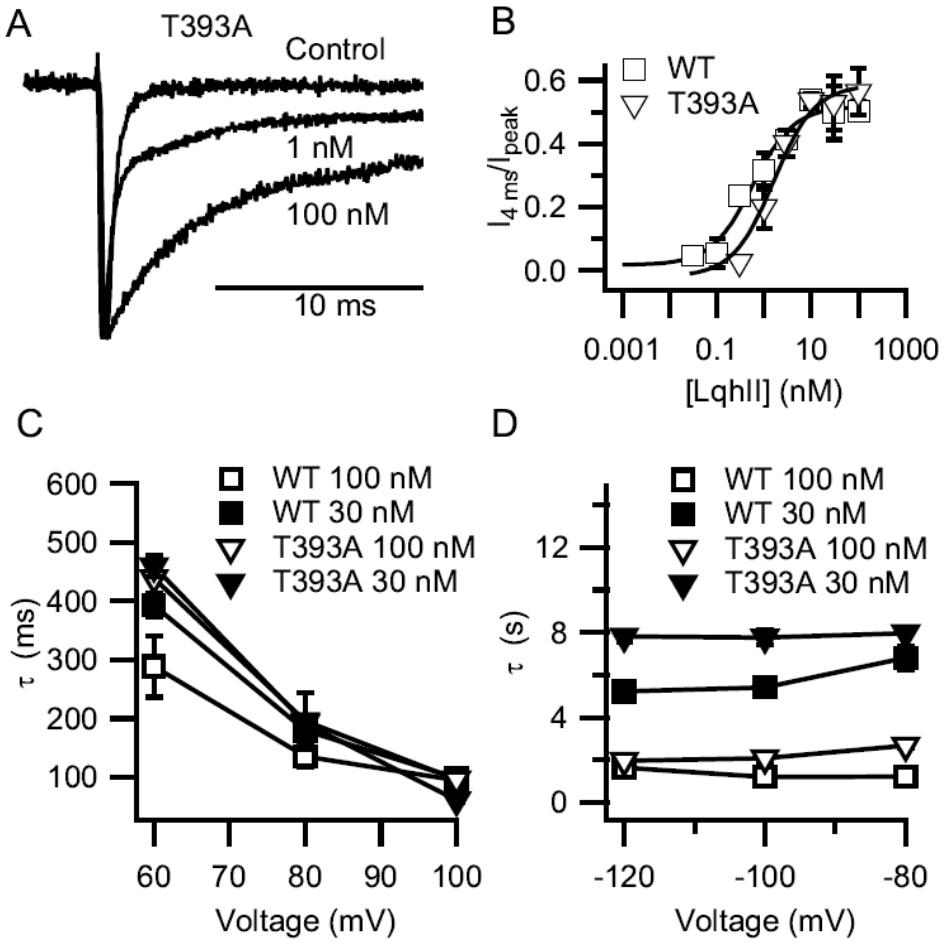

Figure 7 Characterization of mutation T393A in domain ISSII-S6.

(*A*) Normalized current traces during steps to 0 mV from cells expressing T393A channels in the absence (control) and in the presence of 1 nM and 100 nM LqhII. (*B*) Concentration-response relations for LqhII removal of fast inactivation in cells expressing T393A channels (K_d = 1.6±0.5 nM). (*C*) Time constants for LqhII dissociation for T393A and WT channels as a function of potential in the presence of 30 nM and 100 nM LqhII. (*D*) Time constants of association for T393A and WT channels in the presence of 30 nM or 100 nM LqhII.

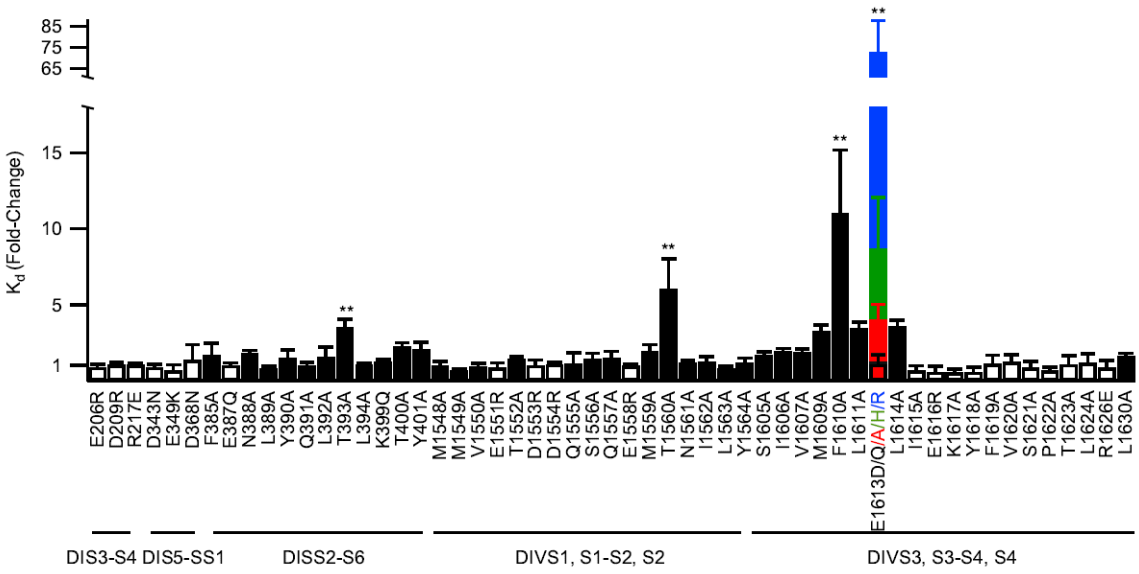

Figure 8 Summary of effects of mutations in domains I and IV on LqhII affinity.

Fold changes in K_d measured either by displacement of bound ^{125}I-LqTxV with unlabeled LqTxV adapted from our previous work (open bars`, *8*) or fold changes in K_d as determined using electrophysiology experiments described here in Results (n= 2-13, filled bars). Different substitutions for E1613 are shown as stacked bars of different colors. Ala and Gly residues (A396, A397, G398, G1608 and A1612) were not studied. R395Q and R395H gave no Na^+ current.

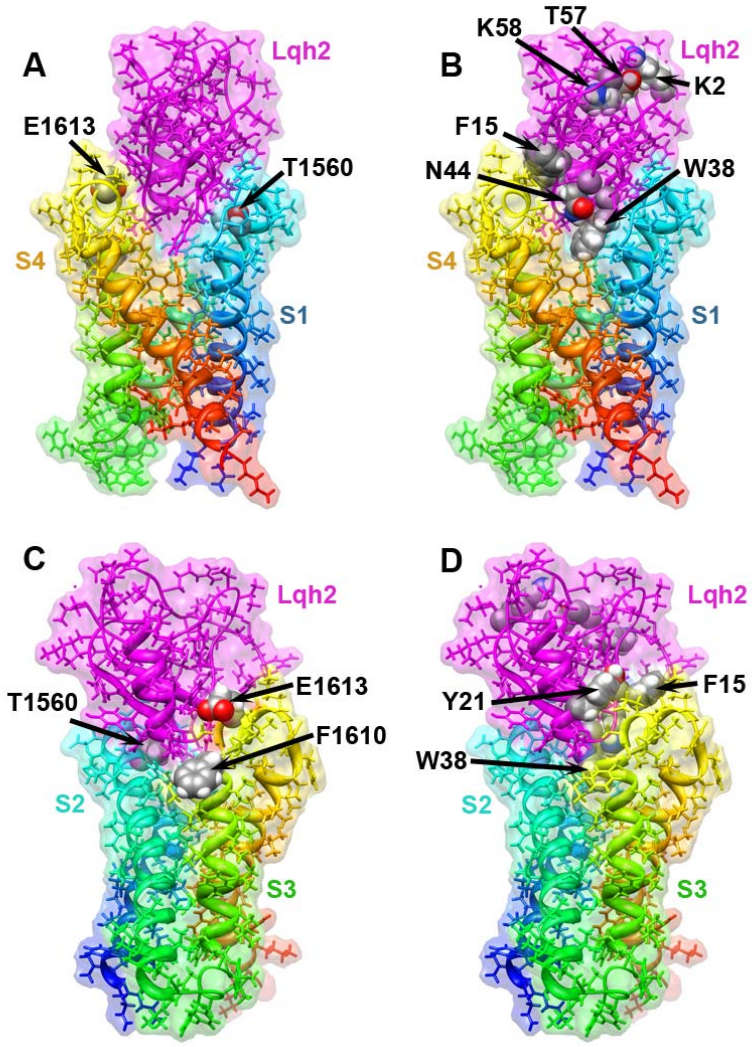

Figure 9 Full atom and molecular surface representation of alpha-scorpion LqhII binding to the voltage-sensing domain IV of $Na_V1.2$.

Segments S1 through S4 of the voltage-sensing domain colored individually and labeled. ***A*** and ***B***, side view of the structural model with the voltage-sensing domain segments S1 and S4 on the front. ***C*** and ***D***, side view of the structural model with the voltage-sensing domain segments and with S2 and S3 on the front (rotated 180° when viewed from the extracellular side of the membrane compared to orientation shown in panels A and B). Side chains of key residues for LqhII-$Na_V1.2$ interaction are shown in spacefilling representation and all other side chains shown in stick representation. A probe radius of 1.4 Å was used to scan the molecular surface of each structural model. This figure was generated using Chimera (*94*).

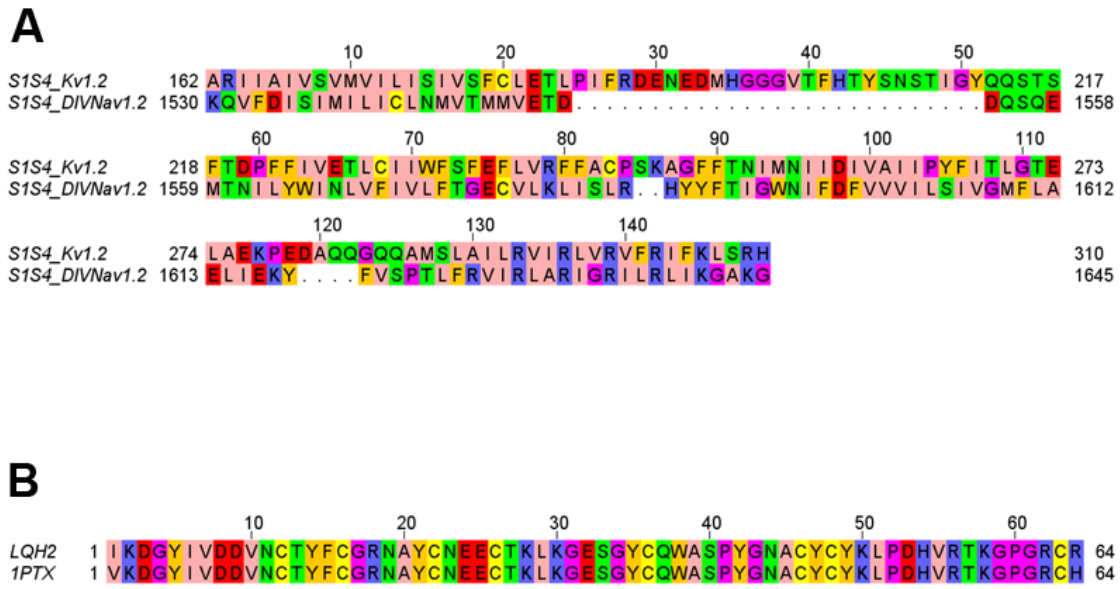

Figure 10 Sequence alignment for voltage-sensing domain IV of $Na_V1.2$ and alpha-scorpion toxins.

A, Sequence alignment between the voltage-sensing domain IV of $Na_V1.2$ and voltage-sensing domain of $K_V1.2$ channel. ***B***, Sequence alignment between α-scorpion LqhII toxin and toxin II (pdb code: 1PTX). Residues were colored with Jalview program (*95*) using the Zappo color scheme, where hydrophobic residues (I, L, V, A, and M) are colored pink, aromatic residues (F, W, and Y) are colored orange, positively charged residues (K, R, and H) are colored blue, negatively charged residues (D and E) are colored red, hydrophilic residues (S, T, N, and Q) are colored green, P and G colored magenta, and C is colored yellow.

Table 1. Voltage-dependence of channel activation for WT and mutant channels, before and after treatment with LqhII.

	$V_{0.5}$ Activation (mV)			
[LqhII] (nM)	0[a]	1	10	100
WT[b]	-29.5±3.6	-31.4±2.3	-29.6±3.8	-31.3±4.3
T393A[b]	-27.9±2.9	-33.8±2.8	-36.8±1.0	-37.5±3.4
T1560A[b]	-24.4±2.0	-27.8±3.2	-31.5±2.5	-25.5±1.5
F1610A[b]	-33.6±2.7	-25.1±3.1	-36.1±5.7	-30.8±3.4
E1613A[b]	-33.1±7.8	-27.3±3.8	-31.7±1.7	-30.0±1.1
E1613R[b]	-31.0±5.1	-24.9±3.3	-27.2±5.5	-23.8±0.8

[a] No mutant value in the column as significantly different from WT (Student's T Test, $p>0.05$; n= 2-7)

[b] No value in the column as significantly different from WT or corresponding mutants in the absence of LqhII (Student's T Test, $p>0.05$; n= 2-13)

Table 2. Voltage-dependence of channel fast inactivation for WT and mutant channels, before and after treatment with LqhII.

	$V_{0.5}$ Fast Inactivation (mV)			
[LqhII] (nM)	0	1	10	100
WT	-70.3±1.3	-61.7±3.8[b]	-54.8±2.0[b]	63.1±6.5[a]
T393A	-67.9±1.6[a]	-66.3±5.4[a]	-70.6±5.4[a]	-68.7±11.3[a]
T1560A	-70.9±7.6[a]	-68.3±4.3[a]	-58.4±4.4[b]	-59.5±9.6[a]
F1610A	-83.5±2.07[b]	-80.9±5.0[a]	-73.3±2.9[b]	-73.8±7.1[b]
E1613A	-85.3±4.5[b]	-78.3±4.6[a]	-79.9±0.9[a]	-60.3±4.7[b]
E1613R	-76.0±5.3[a]	-71.5±14.3[a]	-70.8±0.3[a]	-59.2±2.0[b]

Fast inactivation was measured from a holding potential of -100 mV, prepulsed to 0 mV for 100 ms, and then depolarized to potentials from -100 to 0 mV for 10 ms before returning to -100 mV.

[a] No mutant value in the absence of LqhII as significantly different from WT in the absence of LqhII or no value in the presence of 1, 10, or 100 nM LqhII as significantly different from corresponding WT or mutants in the absence of LqhII (Student's T Test, $p>0.05$; n= 2-6)

[b]Mutant value in the absence of LqhII as significantly different from WT in the absence of LqhII or value in the presence of 1, 10, or 100 nM LqhII as significantly different from corresponding WT or mutants in the absence of LqhII (Student's T Test, $p<0.05$; n= 2-7)

Chapter III: A Specific Interaction between the Gating-Module of Sodium Channels and alpha-Scorpion Toxins

Summary

α-Scorpion toxins, including LqhII (*Leiurus quinquestriatus hebraeus toxin II*), bind to the extracellular surface of resting state of the sodium channel and inhibit fast inactivation. Using site-directed mutagenesis, we have identified residues that constitute the functional interaction surfaces of α-scorpion toxin and its receptor site on the voltage-gated sodium channel. α-Scorpion toxin interacts mainly with channel amino acid residues at Thr1560, Phe1610 and Glu1613 of DIV. The bioactive surface of LqhII has recently been shown to be made of a conserved core domain (Phe-15, Arg-18, Trp-38, and Asn-44) and a variable NC domain (Lys-2, Thr-57, Lys-58). In this work, possible interactions were tested by thermodynamic mutant cycle analysis. Single mutations at key amino acid residues important for activity on toxin and sodium channel were constructed by mutagenesis. We have identified an energetic coupling between amino acid residue Phe1610 and Trp38 of LqhII ($\Sigma\Delta\Delta G$ = 2.45 kcal/mol), a residue that is conserved among many α-scorpion toxins. Toxin dissociation was accelerated by depolarization and increased by mutations at both sites, whereas association rates at negative membrane potentials were not changed for mutation at Phe1610, but slightly increased for mutation at Trp38. We also found that T1560 is coupled with R18 and F1610 is coupled with Y47 with ~1kcal/mol on coupling energy. These results constrain the possible orientation of

α-scorpion toxin with respect to the gating-module of DIV in sodium channel and suggest that upon interaction, the core-domain of LqhII is in close proximity to the sodium channel. This further supports the three-dimensional models of the α-scorpion toxin receptor sites.

Introduction

α-Scorpion toxins are single polypeptides crosslinked by four disulfide bridges, which form a highly conserved, tightly-folded core consisting of an α-helix and three strands of β-sheet (*60*). The functional surface on toxin is composed of two distinct domains: a conserved "core domain" formed by residues of the loops connecting the secondary structure elements of the molecule core and a variable "NC-domain " formed by a five-residue turn (residues 8-12) and a C-terminal segment (residues 56-64) (*62, 63, 96*). Substitutions at each functional domain hamper toxin binding, suggesting that toxin activity requires a cooperative interaction obtained upon binding of the two functional domains to their channels sites. However, the detailed interaction between amino acid residues on toxin and voltage sensor is still unsolved at molecular level. Identification of the molecular determinants for binding of toxins that modify activation or inactivation will provide important information about structural mechanisms of channel gating and give insight into design of therapeutic agents that could prevent toxin action. However, our knowledge on how the channel is regulated by toxin binding is not yet detailed enough for a complete structural model of toxin action.

In order to identify pairwise interactions between residues at the toxin-channel interface, we have constructed mutations in the extracellular loops in domains IV on sodium channels and mutations at residues on the core domain of α-scorpion toxin. In this study, we used the formalism of thermodynamic mutant cycle analysis to assess the degree to which these channel mutations interacted with the mutation on the toxin. New amino acid residue interactions were identified between sodium channel and α-scorpion toxins. This information was used to reevaluate the molecular model of the toxin-receptor complex in the resting state generated using the Rosetta Membrane program.

Materials and Methods

LqhII Synthesis.

Production of LqhII, expression in *Escherichia coli*, *in-vitro* folding, and purification of toxin were performed as described previously (*62, 63*).

Site-Directed Mutagenesis.

cDNA encoding the rat $Na_V1.2$ α subunit domain IV and C-terminus was expressed in the JB2 vector. Mutations in the cDNA were made using the Quick-Change mutagenesis kit (Stratagene). Polymerase chain reaction (PCR) reactions were carried out using a Pfu DNA polymerase. DpN1 digestion was used to eliminate methylated template DNA from the PCR products. After PCR purification (Qiagen standard protocol), amplification of the PCR product was conducted by transformation with Super Competent Top 10 *E. coli* followed by 12 h of growth on agar/Luria broth/ampicillin plates. Single colonies were picked and amplified in liquid Luria broth/ampicillin culture. The DNA was isolated

from the bacteria using the Miniprep purification kit (Qiagen). Mutations were verified by DNA sequencing. Mutant cDNAs was subcloned into the pCDM8 vector encoding the entire rat $Na_V1.2$ α subunit. Plasmid DNA was isolated from *E. coli* using the Maxi-plasmid purification kit (Qiagen).

cDNA Transfection.

tsA-201 cells were transiently transfected with cDNA encoding WT or mutant channels and pEBO-pCD8-leu2, a vector encoding the CD8 receptor, by the calcium phosphate method and plated in a 35-mm dish for electrophysiological analysis. Transfected cells were split 10-20 fold on the day following transfection, and electrophysiological recordings were performed 12-24 hours after transfection. Cells coexpressing sodium channel and CD8 antigen were identified by incubation with polystyrene microspheres coated with anti-CD8 antibody (Invitrogen).

Electrophysiological Recording.

Whole cell voltage clamp experiments was performed using solutions that contained 90 mM CsF, 50 mM CsCl, 10 mM CsEGTA, 10 mM NaF, 2 mM $MgCl_2$, 10 mM Hepes (pH 7.4) in the pipette and 70 mM NaCl, 70 mM N-methyl-D-glucamine, 5 mM CsCl, 1.8 mM $CaCl_2$, 1 mM $MgCl_2$, 10 mM glucose, and 10 mM Hepes (pH 7.4) in the bath (*8*). WT and mutant toxins were dissolved in the extracellular solution containing 1mg/mL bovine serum albumin (BSA) to minimize non-specific toxin binding to plasticware, and diluted to the desired concentration. Data collection was initiated 6 min after breaking the cell membrane to obtain the whole cell voltage clamp configuration.

Data Analysis.

Cells were voltage clamped to −100 mV, depolarized to 0 mV to measure the Na^+ current. The dose-response for toxin induced removal of inactivation was measured by plotting the ratio of the current at 4 ms after depolarization to 0 mV over the peak current ($I_{4\ ms}/\ I_{peak}$) as a function of toxin concentration. K_d and Hill coefficients were calculated by fitting the dose-response relation to the Hill equation:

$I_{4\ ms}/\ I_{peak}$ (0 mV) = 1/ 1+(K_d/[toxin]^h)

Where h is the Hill coefficient, [toxin] is the LqhII concentration, and K_d is the toxin affinity to the sodium channel at -100 mV. Maximal toxin concentration used in the experiment is 1μM. For mutations that toxin doesn't reach saturation under the maximal concentration, K_d was estimated by fixing the maximal effect to 0.6 (WT toxin maximal effect) and fit the data by Hill equation. All K_d that are greater than 250 nM are calculated by estimation. All data is reported as mean ± S.E.

The coupling factor (Ω) between the two residues will be calculated as follows.

Ω= [K_d (WT,WT)* K_d (Mut, Mut)]/[K_d (WT, Mut) *K_d (Mut, WT)]

For ease of comparison, we have reported the value of Ω^{-1} when Ω<1.

The coupling energy (ΣΔΔG) value was calculated for each residue pair using the formula:

ΣΔΔG=RTlnΩ

Results

Functionally important amino acid residues on the sodium channel and α-scorpion toxins.

The strategy for determining the architecture of the channel-toxin complex relies on identifying pairwise interactions between residues across the interaction surface. The first step in this analysis is the identification of the set of functionally important residues on the sodium channel and toxin. Figure 11A shows the results of mutagenic scans of residues at the putative interaction surfaces of voltage-gates sodium channels from previous work (*8, 97*). It showed that on the sodium channel the conserved acidic amino acid residues Thr1560 in IVS1-S2, Phe1610 in IVS3 and Glu1613 in IVS3-S4 are involved in binding of α-scorpion toxins (*97*), and subsequent studies showed that analogous amino acid residues are important for binding of other toxins to voltage-gated K^+ and Ca^{2+} channels (*70*). To identify specific interactions between amino acid residues on the sodium channel with α-scorpion toxins, single mutations at key amino acid residues important for activity on rat $Na_V1.2a$ were constructed. WT or mutant $Na_V1.2a$ channels transiently expressed in the embryonic kidney cell line tsA-201 and analyzed by whole-cell voltage clamp. Cells were voltage clamped to −100 mV, depolarized to 0 mV to measure the Na^+ current. K_d was determined by plotting the fraction of conductance remaining at 4 ms after the peak versus toxin concentration (Fig. 11B). Mutants T1560A, F1610A, E1613A and E1613H all had reduced affinity for LqhII (*Leiurus quinquestriatus hebraeus toxin II*) (Fig. 11C), with ~5.4-, ~10-, ~3.6- and ~8-fold increase in K_d compared with WT, respectively. The triple mutant T1560A/F1610A/E1613R caused a

more dramatic rightward shift for the dose-response curve, with a ~240-fold increase in K_d (Fig. 11C).

On the toxin side, a similar mutagenic scan of the surface amino acids of the toxin identified amino acid residues in the core domain, Phe-15, Arg-18, Trp-38, and Asn-44, which are important for binding (Fig. 12A) (*62*). Single mutants F15A, R18A, W38A and N44A in the core domain of LqhII were expressed in recombinant form as described previously (*62*). In this work, we also studied Y47 near the core domain in the β3 sheet by mutating it to Phe. Mutations at these sites cause little structural perturbation of the toxin (*62, 63*), as inferred from the unchanged CD spectra, so the change in K_d likely reflects the change in toxin binding affinity on the channel. We evaluated the effects of mutations in the embryonic kidney cell line tsA-201 by whole-cell voltage clamp.

Fig 12B shows that in the absence of toxin, Na^+ currents activated and inactivated completely within a few milliseconds. LqhII/R18A 30 nM was as effective in slowing inactivation of wild-type channel as 1 nM WT LqhII (Fig. 12A, B), and 300 nM slowed inactivation of most WT channels. R18A reduced the binding affinity on WT sodium channels ~79-fold (Fig. 12D). LqhII/W38A 300 nM was less effective in slowing inactivation than 100 nM WT LqhII (Fig. 12A, C). Even 1 μM W38A LqhII did not reach maximal modification. The W38A mutation reduced the affinity at least 1870-fold (Fig. 12D). Similarly, the results for mutants F15A, N44A and Y47F also revealed a significant reduction in affinity for wild-type channels. The concentration-response curves were shifted to higher concentration, with a K_d ~162-, ~1820-, and ~5-fold, respectively, higher than WT toxin (Fig. 12D). These results are consistent with the

previous conclusion that residues at core domain are an important component for α-scorpion toxins (*62*, *96*).

Specific pair interactions on the sodium channel with α-scorpion toxins.

A method to characterize the interaction between sodium channel and toxin involves the application of thermodynamic mutant cycle analysis (*98-100*). For mutations whose effects on the energetics of binding are independent, the free-energy changes caused by the two single mutations will be additive; their sum will equal the free-energy change caused by the double mutation; and the coupling energy, calculated as the difference between these two values, will be near 0 kcal/mol. In contrast, if the mutated amino acid residues interact, the effects of their mutations will not be independent; the free energy changes will not be additive; and the resulting coupling energy will be equal or greater than 1 kcal/mol. An example is shown in Fig 13A and B, where mutations are made at F1610 on the channel and at position R18 on the toxin. We measured the K_d of WT, single mutant F1610A, R18A and double mutant F1610A/R18A. The dose-response curves of F1610A and R18A were both shifted to the right compared with WT (Fig. 13A). Double mutation F1610A/ R18A further shifted the dose-response to the right, with a ~254-fold increase in K_d (Fig. 13A). Calculation of the coupling free energy ($\Sigma\Delta\Delta G$) from the four K_d values yields a value of 0.66 kcal/mol (Fig. 13A and B). The coupling energy for this mutant pair is significantly less than 1 kcal/mol, indicating two residues function independently.

Another example is shown in Fig 13C and D, where mutations are made at F1610 on the channel and at position W38 on the toxin. The W38A mutation reduced the affinity

~1870-fold. The rightward shift of the dose response curve of W38A on wild-type channel was rescued by also mutating F1610A on the channel (Fig. 13C). The double mutant W38A/F1610A shows only a ~280-fold decrease in K_d (Fig. 13C). Calculation of the coupling free energy from the four K_d values yields a value of 2.45 kcal/mol (Fig. 13C and D). These results indicate F1610 and W38 are energetically coupled.

The K_d values for double mutants at F1610 are summarized in Fig. 13E and its corresponding coupling energy is summarized in Fig. 13F. Of the tested toxin mutations, W38A and Y47 interacted with channel mutation F1610A with an energy equal or significantly greater than one kcal/mol. The coupling energies between F1610A and F15A, R18A, or N44A are all less than 1 kcal/mol. We conclude that channel residue F1610 couples with toxin residues W38 and Y47, but is not significantly coupled to other residues tested. These results show for the first time that one amino acid residue at the core domain of α-scorpion toxin is in close proximity to the voltage sensor of sodium channel. W38 is highly conserved across all the α-scorpion toxin family (*63*). These results may reflect a general aromatic-aromatic interaction between sodium channel and toxin and may enable recognition of receptor site 3 by all α-scorpion toxins.

Figure 14 shows the collection of K_d for double mutants and its corresponding coupling energy for T1560 and E1613 studied in this work. The coupling energy ($\Sigma\Delta\Delta G$) was less than 1 kcal/mol for all these mutant cycles except for T1560A/R18A. These results indicate T1560 is energetically coupled with R18 and E1613 is not energetically coupled with residues we studied on the toxin. The pair interactions with Glu1613 in S3-S4 loop need further experiments to be identified.

Kinetics of Dissociation of LqhII.

Binding of α-scorpion toxins is reversed by strong depolarizations that activate the voltage sensor (*8, 74, 97*). Cells expressing WT and F1610A channel were voltage clamped to −100 mV to allow maximum binding, and then depolarized to 100 mV for 0.1 to 1,024 ms to induce dissociation, hyperpolarized to −100 mV for 20 ms to reverse inactivation, and depolarized to 0 mV for measurement of Na^+ current (Fig. 15A). For WT channels in the presence of 100 nM LqhII, progressively longer depolarizations caused faster and more complete Na^+ channel inactivation, indicating LqhII dissociation (Fig. 15A). Dissociation of toxin and loss of toxin action were virtually complete after a 256-ms depolarization to 100 mV (Fig. 15B). For WT in the presence of 100 nM LqhII, the dissociation rate constant was $10.5 \pm 0.4\ s^{-1}$ at 100 mV.

The same protocol was used to measure the dissociation rate for single mutant F1610A, W38A and double mutant F1610A/W38A (Fig. 15B and C) at 100 nM or 1μM toxin. 1 μM W38A toxin was used because the mutant toxin effect at 100 nM is too low to measure the rate accurately. The WT had the slowest dissociation. Channel mutation F1610A and toxin mutation W38A increased the rate constant by ~6.7- and ~5.0-fold, respectively (Fig. 15B and C). The effect was even greater for F1610A/W38A, with ~21.5-fold increase in rate constant. The time course of toxin dissociation was also determined in the presence of 30 nM WT or 300 nM W38A toxin (Fig. 15D). The dissociation rate constants showed little or no concentration-dependence (Fig. 15D), indicating that the dissociation step is a state-dependent, unimolecular reaction. Consistent with previous data (*8, 97*), the dissociation rate constants for WT and all three

mutant combinations were voltage-dependent (Fig. 17A), with more rapid dissociation during stronger depolarization.

Kinetics of Reassociation of LqhII.

The rates of toxin association were assessed for WT and mutants using a 200-ms prepulse to 100 mV to cause toxin dissociation, followed by progressively longer hyperpolarizing pulses to -100 mV to allow toxin rebinding, and a final test depolarization to 0 mV to assess LqhII action (Fig. 16A). For WT channels, toxin dissociated during the prepulse, as indicated by the rapid inactivation when only 50 ms were allowed for rebinding (Fig. 16B). Toxin gradually rebound after longer repolarizations with complete reassociation at 12.8 s (Fig. 16B). For WT in the presence of 100 nM LqhII, the reassociation rate constant was $0.83 \pm 0.12\ s^{-1}$ at -100 mV.

The same protocol was used to measure the association rate for single mutant F1610A, W38A and double mutant F1610A/W38A at 100 nM or 1 μM toxin (Fig. 16B and C). The rate constants for toxin binding to F1610A were similar to WT (Fig. 16B). The rate constant for W38A was measured using 1 μM, a 10-fold higher toxin concentration than WT toxin, however, the rate constant for W38A showed ~20.7-fold increase compared to corresponding values for 100 nM WT toxin (Fig. 16C). It means that the mutation W38A increased the toxin association rate at hyperpolarized potentials. The rate constant of toxin association showed a similar increase, about ~22.6-fold, for double mutation F1610A/W38A (Fig. 16C) at 1 μM toxin. Thus, there is no effect of F1610A but substantially increased rate of W38A association at hyperpolarized potentials. The time course of toxin reassociation was also determined in the presence of 30 nM WT or 300

nM W38A toxin (Fig. 16D). The association rate constants showed strong concentration-dependence (Fig. 16D), indicating that the association step is a bimolecular reaction. Consistent with previous data (*8, 97*), there was little or no voltage-dependence for toxin reassociation (Fig. 17B).

Discussion

Previous work shows that α-scorpion toxins bind mainly on the S1-S2 and S3-S4 loops in domain IV with a secondary binding site on S5-S6 loop in domain I (*97*). In this work, we found that removing the primarily binding site in domain IV by triple mutants T1560A/F1610A/E1613R caused a ~240-fold decrease in binding affinity. Mutation on any of these residues diminish the interaction and thereby the activity. The overall effect is additive with the triple mutant, indicating that the primary binding site is removed by the triple mutant.

Mutant cycle analysis was first introduced to analyze interactions of substrates and regulators with enzymes (*101*) and has been extensively used subsequently to study mutagenesis and structure-function relationships of many proteins (*98-100*). This method was used to identify a specific ion pair interaction between site 3 sea anemone toxin anthopleurin B (ApB) and cardiac sodium channel (*100*). We use this technique to explore the interactions of wild-type toxin with wild-type channels, and combinations of toxin mutated at the putative interaction residue with the channels mutated at the putative-interacting residue. Channel residue F1610 and toxin residue W38 display a coupling energy of $\Sigma\Delta\Delta G$ = 2.45 kcal/mol. This coupling energy is within the range predicted for aromatic-aromatic interactions (1-2 kcal/mol) (*102*) and contributes to

channel-toxin stability. It also indicates two amino acid residues are separated by 4Å or less. Since W38 is highly conserved across all the α-scorpion toxin family (*63*) and F1610 is conserved in most of sodium channel subtypes ($Na_V1.1$, $Na_V1.2$, $Na_V1.3$, $Na_V1.6$ and $Na_V1.7$), these results may reflect a general aromatic-aromatic interaction between sodium channel and toxin and may enable recognition of receptor site 3 by all α-scorpion toxins.

Our molecular model, generated in the most stable channel conformation with LqhII, also suggested that the toxin core domain interacts with the gating module of DIV (*96, 97*). However, in the model, the side chain of Phe1610 points away from the bound LqhII. A slightly unwound in the IVS3 helix beginning at Phe1610 allows its interaction with Trp38 in the core domain of LqhII. This unwound conformation may be favorable for DIV voltage sensor in the resting state of the channel.

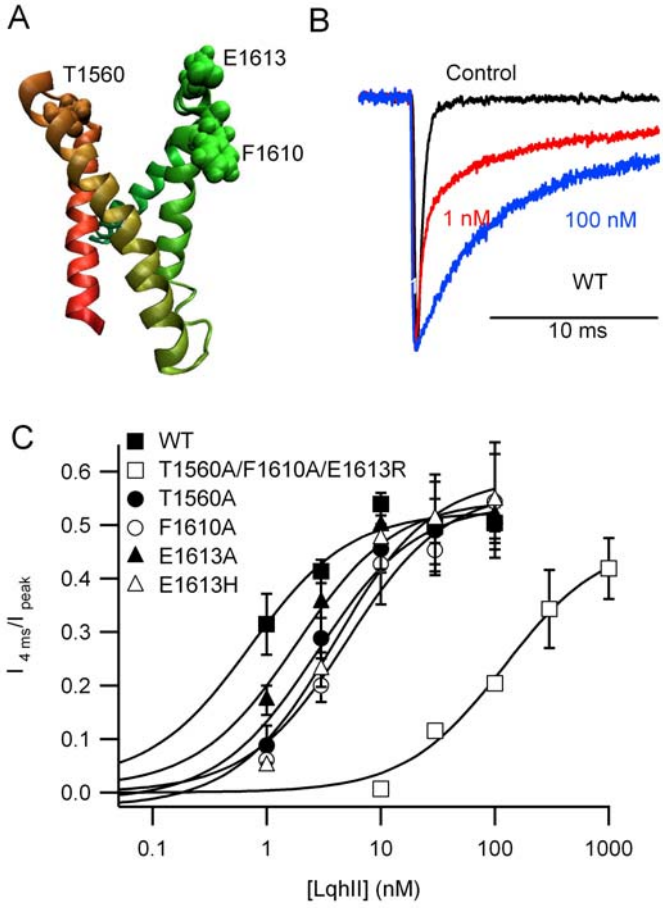

Figure 11 Amino acid residues mutated for mutant cycle analysis on sodium channel.

(A) Image showing the positions of T1560, F1610 and E1613 (space-filling models) in the voltage-sensing domain IV of $Na_V1.2a$ at resting state. This model is generated using Rosetta docking method as previous described (*97*). (B). Normalized voltage-clamp current traces from tsA-201 cells expressing WT channels in the absence (Control, black) and in the presence of 1 nM (red) and 100 nM (blue) LqhII. Cells expressing $Na_V1.2a$ channel were held at −100 mV and Na^+ currents were elicited with a 30-ms step to 0 mV. (C) Concentration-response relations for LqhII removal of fast inactivation in cells expressing WT and mutant channels. WT (K_d = 0.5 ± 0.05 nM, n = 3–8), T1560A (K_d = 2.7 ± 0.8 nM, n = 3–5), F1610A (K_d = 5.0 ± 1.8 nM, n = 3–6), E1613A (K_d = 1.8 ± 0.4 nM, n = 3–5), E1613H (K_d = 4.0 ± 0.5 nM, n = 2–4) and T1560A/F1610A/E1613R (K_d = 120 ± 22 nM, n = 2–3).

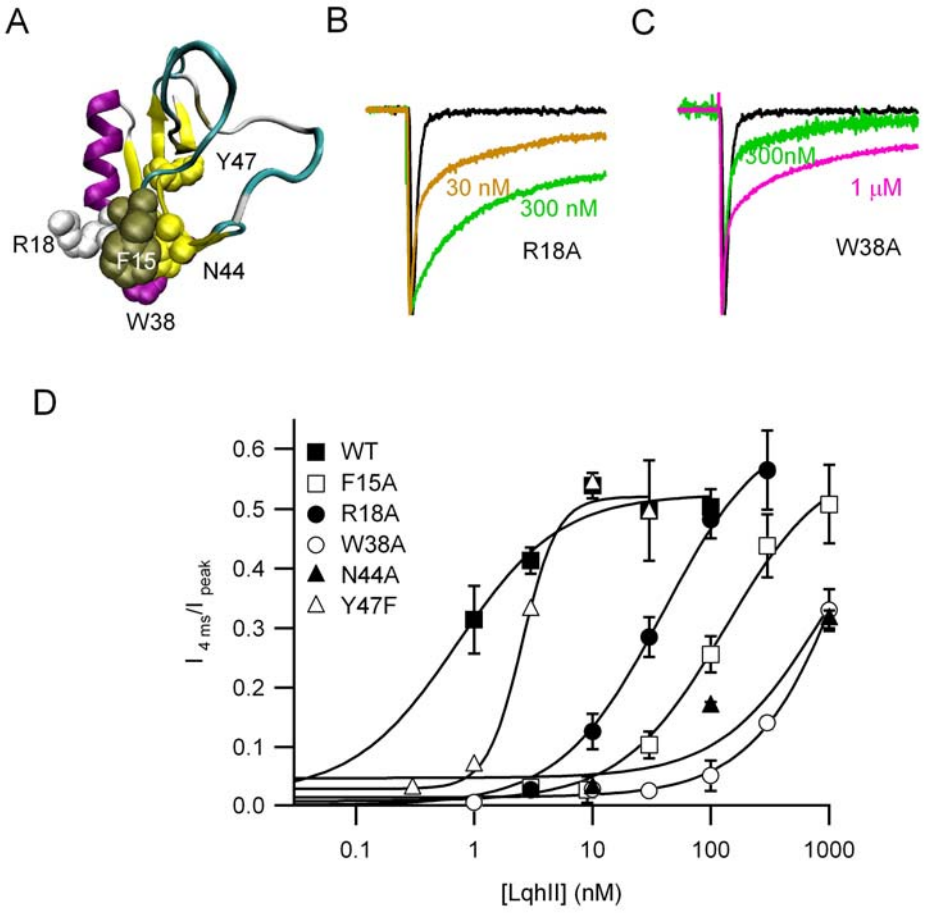

Figure 12 Amino acid residues mutated for mutant cycle analysis on LqhII.

(A) Modeling of the LqhII structure based on the known structure of Aah2 (PDB code 1aho). Residues studied in this work, F15, R18, W38, N44 and Y47 are space-filled. (B and C). Normalized voltage-clamp current traces from tsA-201 cells expressing WT channels in the absence (Control, black) and in the presence of 30 nM (orange), 300 nM (green), or 1 μM LqhII (pink). Cells expressing $Na_V1.2a$ channel were held at −100 mV and Na^+ currents were elicited with a 30-ms step to 0 mV. (D) Concentration-response relations for WT and mutant LqhII removal of fast inactivation in cells expressing WT channels. F15A (K_d = 131 ± 25 nM, n = 3–5), R18A (K_d = 39.3 ± 6.8 nM, n = 3–6), W38A (K_d = 937 ± 79 nM, n = 2–3), N44A (K_d = 912 ± 381 nM, n = 2) and Y47F (K_d = 2.5 ± 0.3 nM, n = 3–4).

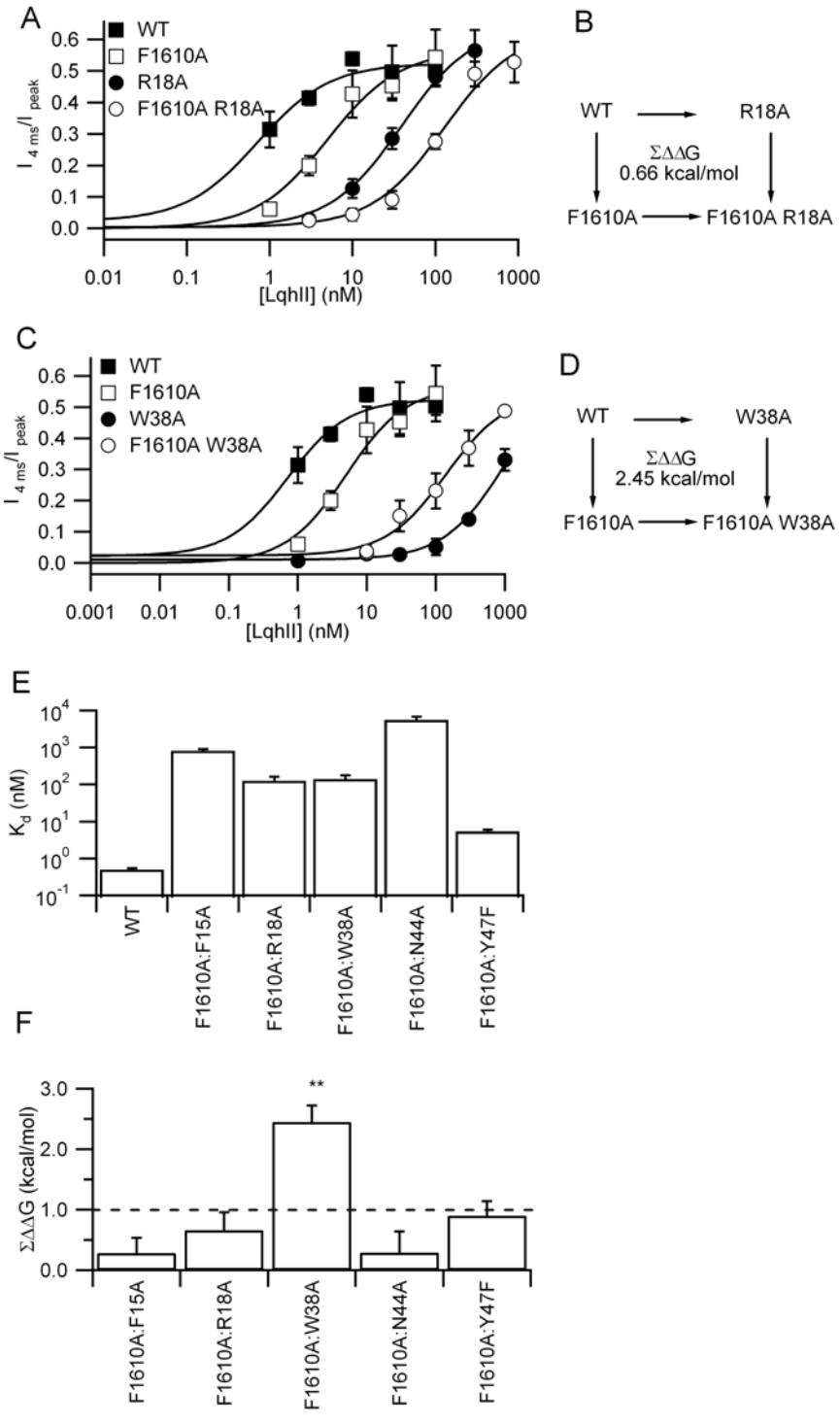
A
WT
F1610A
R18A
F1610A R18A
I 4 ms/I peak
[LqhII] (nM)
B
WT
R18A
ΣΔΔG
0.66 kcal/mol
F1610A
F1610A R18A
C
WT
F1610A
W38A
F1610A W38A
I 4 ms/I peak
[LqhII] (nM)
D
WT
W38A
ΣΔΔG
2.45 kcal/mol
F1610A
F1610A W38A
E
Kd (nM)
WT
F1610A:F15A
F1610A:R18A
F1610A:W38A
F1610A:N44A
F1610A:Y47F
F
ΣΔΔG (kcal/mol)
**
F1610A:F15A
F1610A:R18A
F1610A:W38A
F1610A:N44A
F1610A:Y47F

Figure 13 Mutant cycle analysis at F1610.

(A and C). Concentration-response relations for LqhII removal of fast inactivation in cells expressing WT and F1610A channels. F1610A/R18A (K_d = 127 ± 37 nM, n = 3–7), F1610A/W38A (K_d = 140 ± 38 nM, n = 3–6). (B and D) The calculated coupling energies (ΣΔΔG) for F1610, R18 and F1610, W38 residue pair. (C) K_d for double mutants measured as determined using electrophysiology experiments described in Results (n = 3–6). (D) Coupling energy (ΣΔΔG) for each residue pair as described in Methods. Mean ± SEM.

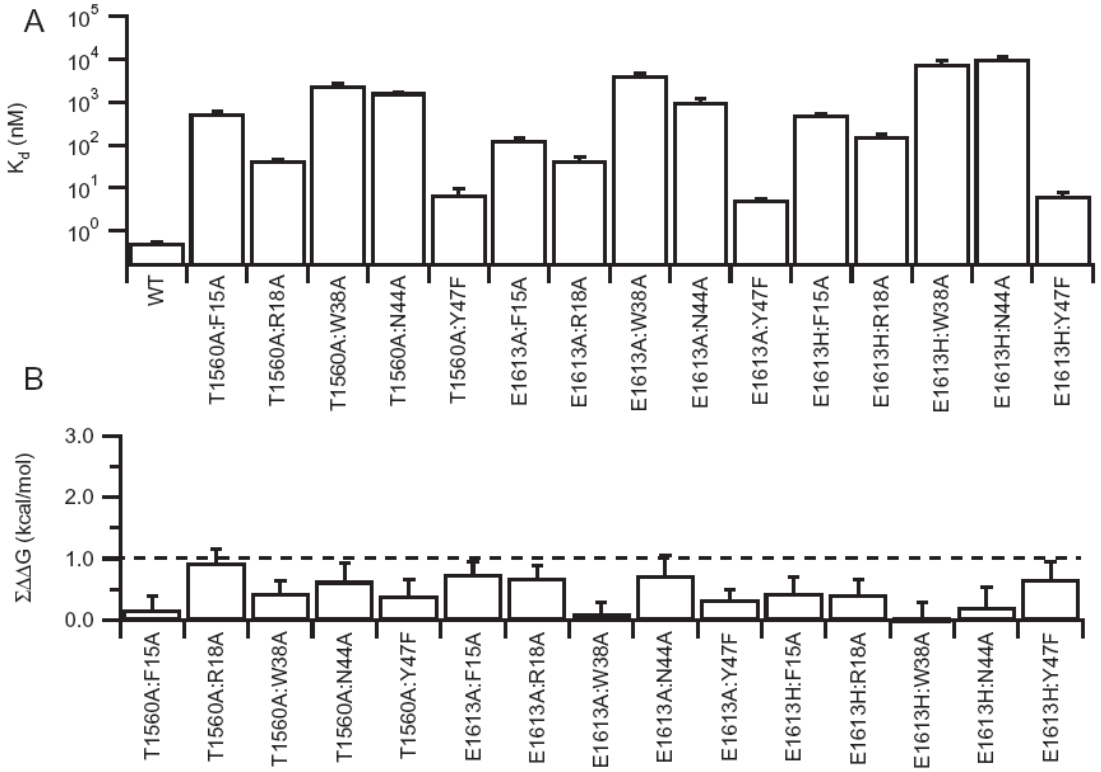

Figure 14 Mutant cycle analysis at T1560 and E1613.

(A) K_d for double mutants measured as determined using electrophysiology experiments described in Results (n = 3–6). (B) Coupling energy (ΣΔΔG) for each residue pair as described in Methods. Mean ± SEM.

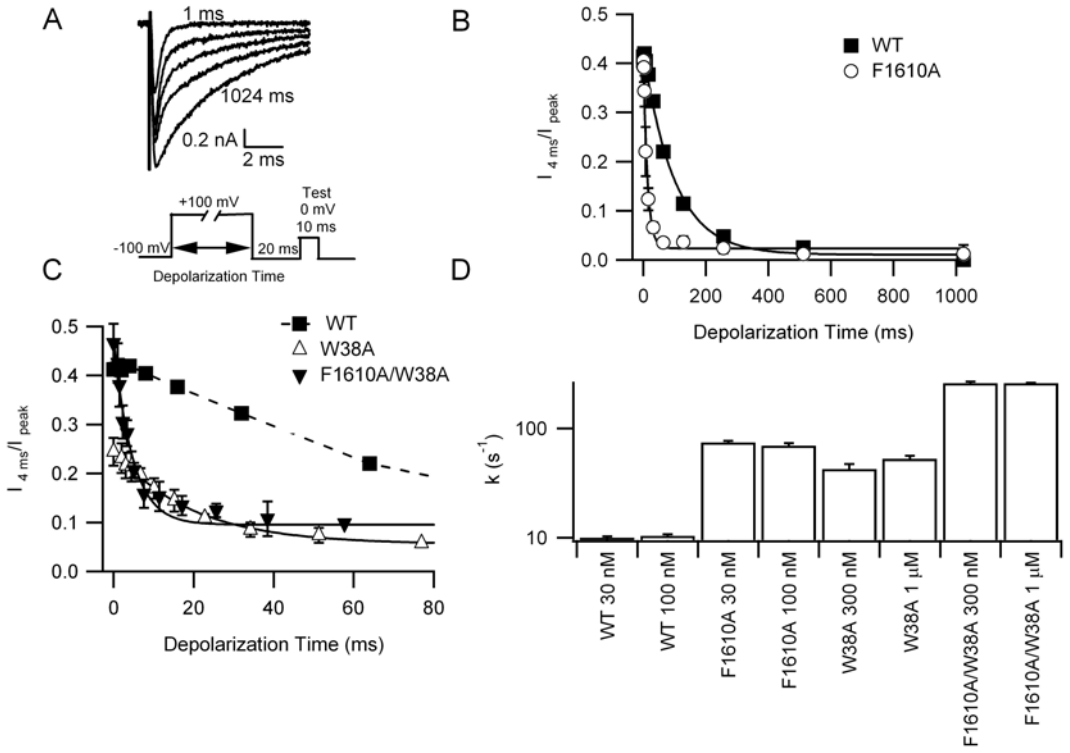

Figure 15 Dissociation rates of LqhII.

(A) Traces demonstrating time-dependent dissociation of LqhII at 100 mV. Cells expressing WT and mutant $Na_V1.2$ channels were incubated in 100 nM LqhII for 6 min at a holding potential of −100 mV to allow binding. The rate of toxin dissociation was determined with the illustrated pulse paradigm by stepping to a depolarizing pulse of 100 mV, for 0.1 to 1,024 ms, returning to −100 mV for 20 ms to allow recovery from fast inactivation and then assessing the effect of the depolarizing pulse with a 10-ms test pulse to 0 mV (test). (B) Time course of dissociation of 100 nM WT LqhII from cells expressing WT and F1610A channels. WT ($k = 10.5 \pm 0.4\ s^{-1}$, n = 3) and F1610A ($k = 69.7 \pm 4.1\ s^{-1}$, n = 4). (C) Time course of dissociation of 1µM W38A LqhII from cells expressing WT and F1610A channels. W38A ($k = 52.7 \pm 3.6\ s^{-1}$, n = 5) and F1610A/W38A ($k = 255 \pm 3\ s^{-1}$, n = 3). Rate constants were determined by fits of monoexponential functions to the data. (D) Rate constants of dissociation as a function of concentration for WT and F1610A.

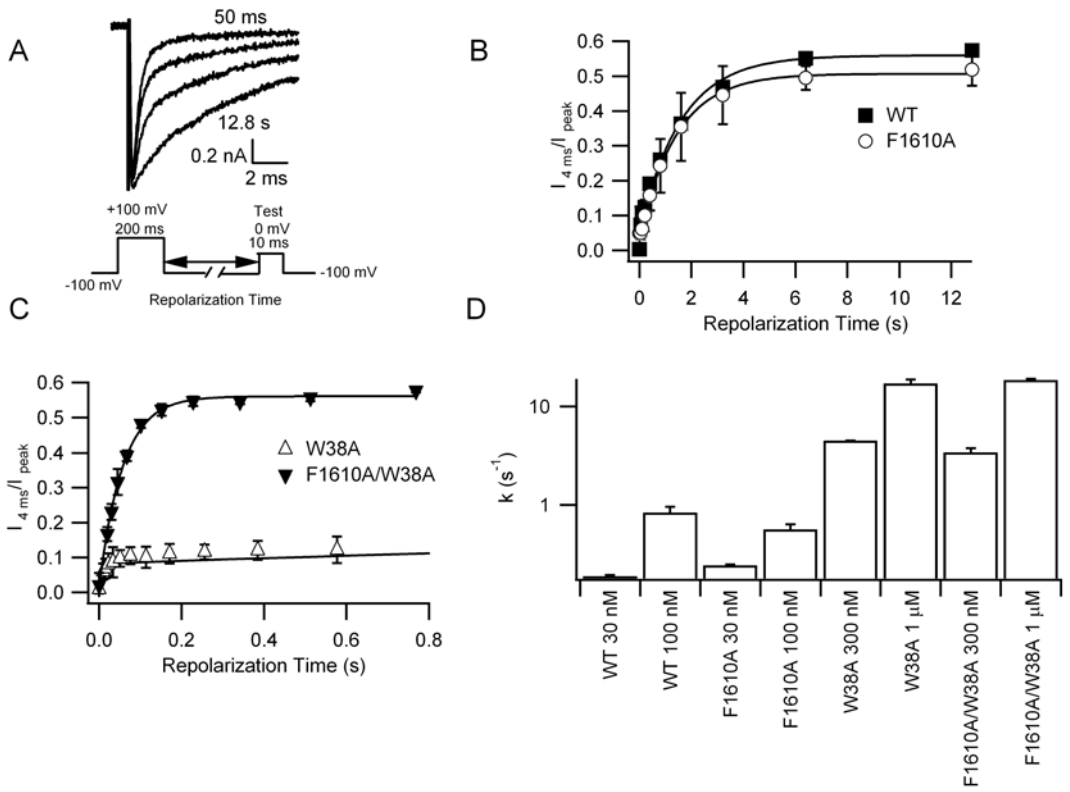

Figure 16 Association rates of LqhII.

(A) Traces demonstrating time-dependent dissociation of LqhII at -100 mV. Cells expressing WT and mutant $Na_V1.2$ channels were incubated in 100 nM LqhII. Toxin was dissociated from the channel using a 200-ms depolarization to 100 mV. The rate of toxin association was measured by hyperpolarizing to −100 mV for increasing times. The effect of repolarization on toxin action was assessed with a 10-ms test pulse to 0 mV (test). (B) Time course of asssociation of 100 nM WT LqhII from cells expressing WT and F1610A channels. WT ($k = 0.83 \pm 0.12$ s^{-1}, $n = 3$) and F1610A ($k = 0.56 \pm 0.07$ s^{-1}, $n = 3$). (C) Time course of asssociation of 1 µM W38A LqhII from cells expressing WT and F1610A channels. W38A ($k = 17.2 \pm 1.7$ s^{-1}, $n = 4$) and F1610A/W38A ($k = 18.8 \pm 0.5$ s^{-1}, $n = 3$). (D) Rate constants of association as a function of concentration for WT and F1610A.

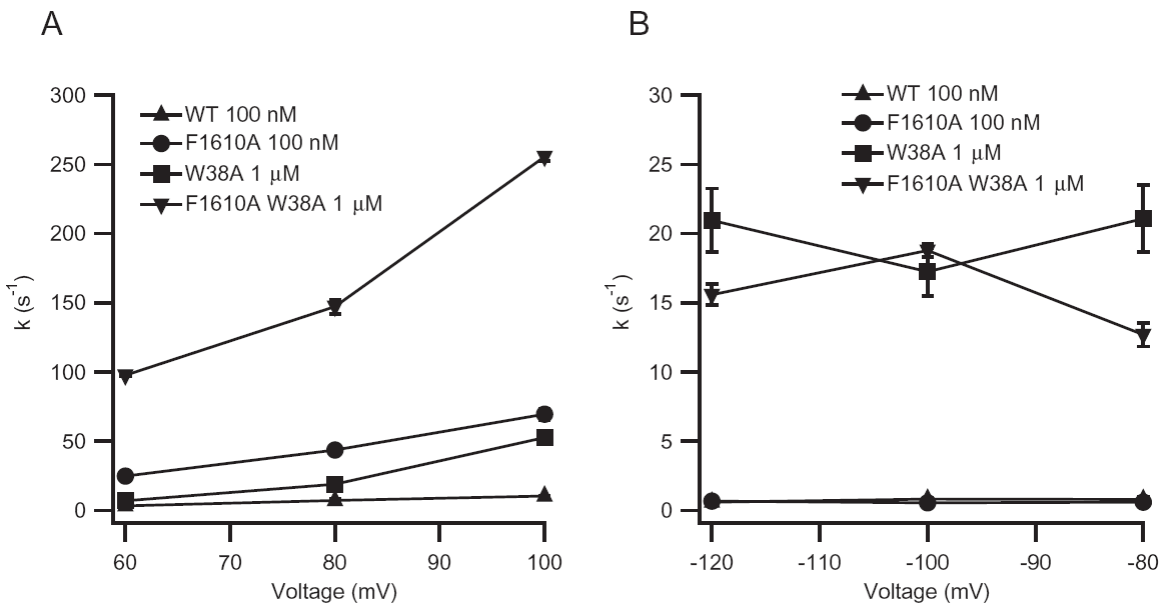

Figure 17 Rate constants of dissociation and association.

(A) Rate constants of dissociation as a function of voltage for WT, F1610A, W38A and F1610A/W38A channels. (B) Rate constants of association as a function of voltage for WT, F1610A, W38A and F1610A/W38A channels.

Chapter IV: Block of alpha-Scorpion Toxins Action on Sodium Channels by Ranolazine

Summary

α-Scorpion toxins, including LqhII (*Leiurus quinquestriatus hebraeus toxin II*), bind to the extracellular surface of resting state of the sodium channel and inhibit fast inactivation. These toxins can increase the late Na^+ current. We hypothesized that the antianginal and anti-ischemic drug, ranolazine will inhibit the late Na^+ current induced by α-scorpion. Whole cell Na^+ current was recorded from CHO cells expressing the rat $Na_V1.2$ WT channels. Ranolazine attenuated both peak and late Na^+ current in the presence of 100 nM α-scorpion toxin, with a 50% inhibitory concentration (IC_{50}) 334 ± 2.6 μM and 102 ± 10.7 μM, respectively. The results demonstrate that ranolazine reduces late Na^+ current induced by α-scorpion toxin and has antagonist effect against α-scorpion toxin. Consistent with this effect on sodium channels, ranolazine reduces the lethal paralytic effects of LqhII in mice.

Introduction

α-Scorpion toxins are single polypeptides crosslinked by four disulfide bridges, which form a highly conserved, tightly-folded core consisting of an α-helix and three strands of β-sheet (*60*). These toxins bind to the extracellular domain on the sodium channel and inhibit channel fast inactivation. α-Scorpion toxins bind in a state-dependent manner,

with high affinity for the resting state. Once bound, these toxins impair channel fast inactivation, which can cause an increase of late Na^+ current. This small current increase may cause a prolongation of action potential duration (APD).

Ranolazine is an antianginal and anti-ischemic drug that is used in patients with chronic angina (*103*, *104*). It blocks sodium channel activity in a manner that resembles local anesthetic block of sodium channels: block is use-dependent (*105*). It has been suggested that the drug might interact with the local anesthetic receptor site, which lines the inner mouth of the channel pore (*103*). This drug is particular interest because it has been shown to reduce late Na^+ channel current, attenuate the prolongation of APD and suppress the development of arrhythmogenic early after depolarization in a model of LQT-3 (long QT syndrome type 3) in which sustained Na^+ channel activity is induced by sea anemone toxin (*106*). This observations led us to hypothesize that ranolazine can block late Na^+ current induced by α-scorpion toxins. Using CHO cells stably expressing rat $Na_V1.2a$ WT channels, we show that ranolazine can block α-scorpion toxin action on sodium channels and stabilize the fast inactivation state..

Materials and Methods

LqhII Synthesis.

Production of LqhII, expression in *Escherichia coli*, *in-vitro* folding, and purification of toxin were performed as described previously (*62*, *63*).

Cell line.

Stable CHO cell lines expressing rat brain $Na_V1.2a$ channels were made previously (*107*). To prepare cells for electrophysiological recording, we incubated cells in the 100 mm cuvette dishes until 90% confluence. We aspirated media from cell culture plates and washed them twice with 15 mL PBS and then added 2 ml Trypsin-EDTA solution. We incubated at 37 ^{O}C for 2 minutes until cells began to dislodge the plate. The trypsinization reaction was stopped by adding 2 mL of media to each plate. The cells were sedimented at 2000 rpm for 2 min at room temperature. The supernatant was aspirated and cells were resuspended in 1 mL extracellular solution.

Electrophysiological Recording.

Electrophysiological recordings were performed in whole-cell voltage clamp mode using the automated patch clamp workstation Patchliner (Nanion Instruments). Intracellular solutions contained 50 mM CsCl, 10 mM NaCl, 60 mM CsF, 20 mM EGTA, 10 mM Hepes (pH 7.2) and extracellular solutions contained 140 mM NaCl, 4 mM KCl, 1 mM $MgCl_2$, 2 mM $CaCl_2$, 5 mM D-Glucose monohydrate, and 10 mM Hepes (pH 7.4). WT toxins were dissolved in the extracellular solution containing 1mg/mL bovine serum albumin (BSA) to minimize non-specific toxin binding to plasticware. Ranolazine was purchased from Sigma-Aldrich and diluted to the desired concentration in the extracellular solution.

Data Analysis.

Cells were voltage clamped to −100 mV, depolarized to 0 mV to measure the Na^+ current. The dose-response was measured by plotting the peak current after depolarization to 0 mV or late current at 30 ms after depolarization as a function of

ranolazine concentration. IC_{50} and Hill coefficients were calculated by fitting the dose-response relation to the Hill equation:

$I_{peak\ or\ late}/ I_{peak\ or\ late}$ (100 nM LqhII) = 1/ [1+([Ranolazine]/IC_{50})^h]

Where h is the Hill coefficient, [Ranolazine] is the ranolazine concentration, and IC_{50} is the ranolazine concentration that causes 50% block. All data is reported as mean ± S.E.

Results

Ranolazine block of α-scorpion toxin action on rNa$_V$1.2a channels

Stable CHO cell lines expressing rat brain $Na_V1.2a$ channels were made previously (*107*) and analyzed by whole-cell voltage clamp. Cells were voltage clamped to −100 mV, depolarized to 0 mV to measure the Na^+ current, and tested for modification by LqhII (*Leiurus quinquestriatus hebraeus, toxin II*) and ranolazine by perfusion. In the absence of toxin, Na^+ currents activated and inactivated completely within a few milliseconds (Fig. 18A). Perfusion of 100 nM LqhII slowed inactivation of WT channels as well as increased the peak current by 17%. Perfusion of 100 μM ranolazine in the presence of 100 nM LqhII, reduced both the peak and late current. Both currents are reduced more significantly after perfusion 300 μM or 1 mM ranolazine.

α-Scorpion toxin affected channel function mainly by removing channel fast inactivation. To compare the level of ranolazine block of the late current caused by LqhII specifically, we normalized the current traces in Fig. 18A to the peak current (Fig 18B). Ranolazine blocks the late current caused by LqhII in a concentration-dependent manner.

This result shows that ranolazine can block of α-scorpion toxin action on $Na_V1.2$ channels selectively.

To determine the IC_{50}, both the peak current and the fraction of conductance remaining at 30 ms after the peak were plotted versus ranolazine concentration (Fig. 18C). These data were fit with a Hill equation. From this analysis, the IC_{50} for ranolazine block was estimated to be 334 ± 2.6 μM with a Hill coefficient of 1.13 ± 0.01 for the peak current and 102 ± 10.7 μM with a Hill coefficient of 1.84 ± 0.34 for the late current. The leftward shift of the dose-response curve for the late current means that ranolazine is more effective in blocking the late current than the peak current. The IC_{50} of ranolazine block was also determined in the presence of 10 nM, 30 nM and 300 nM LqhII (Fig. 18D). The IC_{50} for both peak and late current showed little concentration-dependence, indicating that the ranolazine is a non-competitive antagonist against LqhII.

There was no significant shift for the voltage-dependence of channel activation and fast inactivation before and after perfusion of 100 μM ranolazine in the presence of 100 nM LqhII (Fig 19), except that the peak currents were reduced at all depolarized potentials measured after addition of ranolazine.

Discussion

α-Scorpion toxins mainly affect channel function by slowing the channel fast inactivation. An antagonist against α-scorpion toxins action should restore the channel fast inactivation partially or completely. Ranolazine reduces both the peak and late Na^+ current in the presence of α-scorpion toxins, but preferentially it inhibits late Na^+ current

with 102 ± 10.7 μM in IC_{50}. These data further suggest that ranolazine might be useful to recover the neuromuscular paralysis induced by α-scorpion toxins.

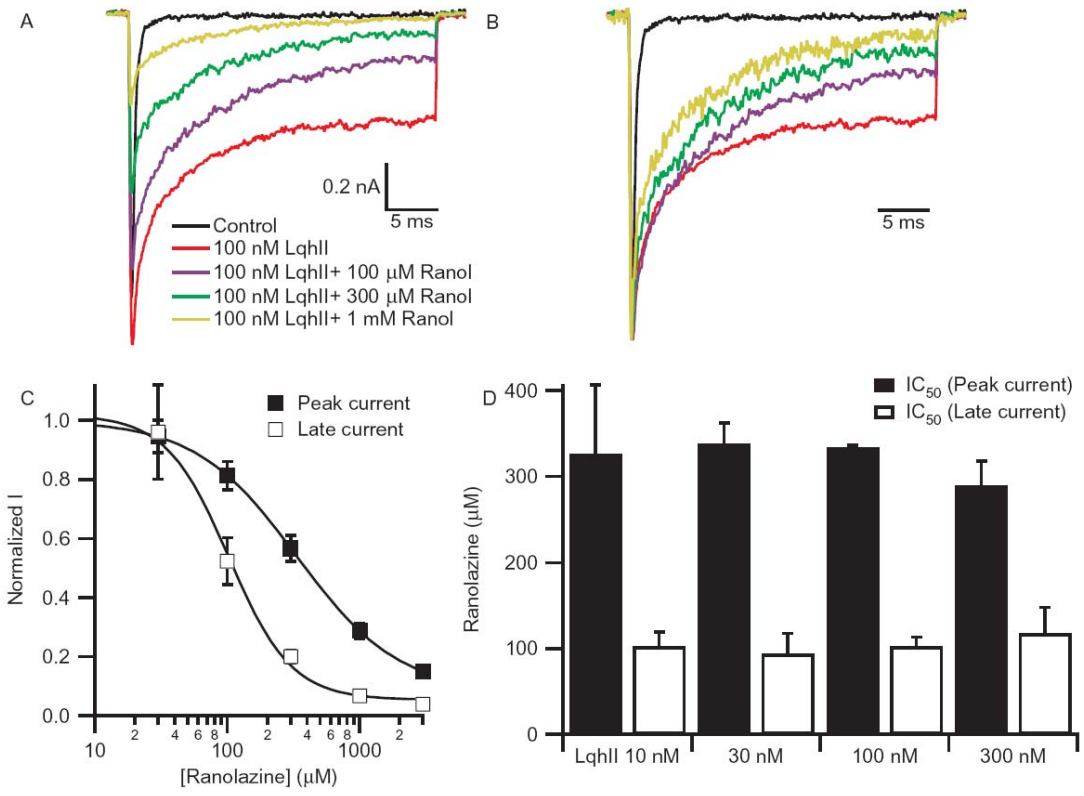
A
B
0.2 nA
5 ms
5 ms
Control
100 nM LqhII
100 nM LqhII+ 100 µM Ranol
100 nM LqhII+ 300 µM Ranol
100 nM LqhII+ 1 mM Ranol
C
Peak current
Late current
Normalized I
1.0
0.8
0.6
0.4
0.2
0.0
10
100
1000
[Ranolazine] (µM)
D
IC50 (Peak current)
IC50 (Late current)
Ranolazine (µM)
400
300
200
100
0
LqhII 10 nM
30 nM
100 nM
300 nM

Figure 18 Block of alpha-scorpion toxin LqhII function by ranolazine.

(A) Voltage-clamp current traces from CHO cells expressing rat $Na_V1.2a$ channels in the absence (Control, black) and in the presence of 100 nM LqhII before (red) and after perfusion 100 μM (purple), 300 μM (green) or 1 mM (yellow) ranolazine. Cells expressing $Na_V1.2a$ channel were held at −100 mV and Na^+ currents were elicited with a 30-ms step to 0 mV. (B) Normalized voltage-clamp current traces in (A). (C) Concentration-response relations for ranolazine block of peak and late current in the presence of 100 nM LqhII in cells expressing WT channels. IC_{50} (Peak current) = 334 ± 2.6 μM and IC_{50} (Late current) = 102 ± 10.7 μM, n = 3. (D) IC_{50} of peak current and IC_{50} of late current as a function of LqhII concentration.

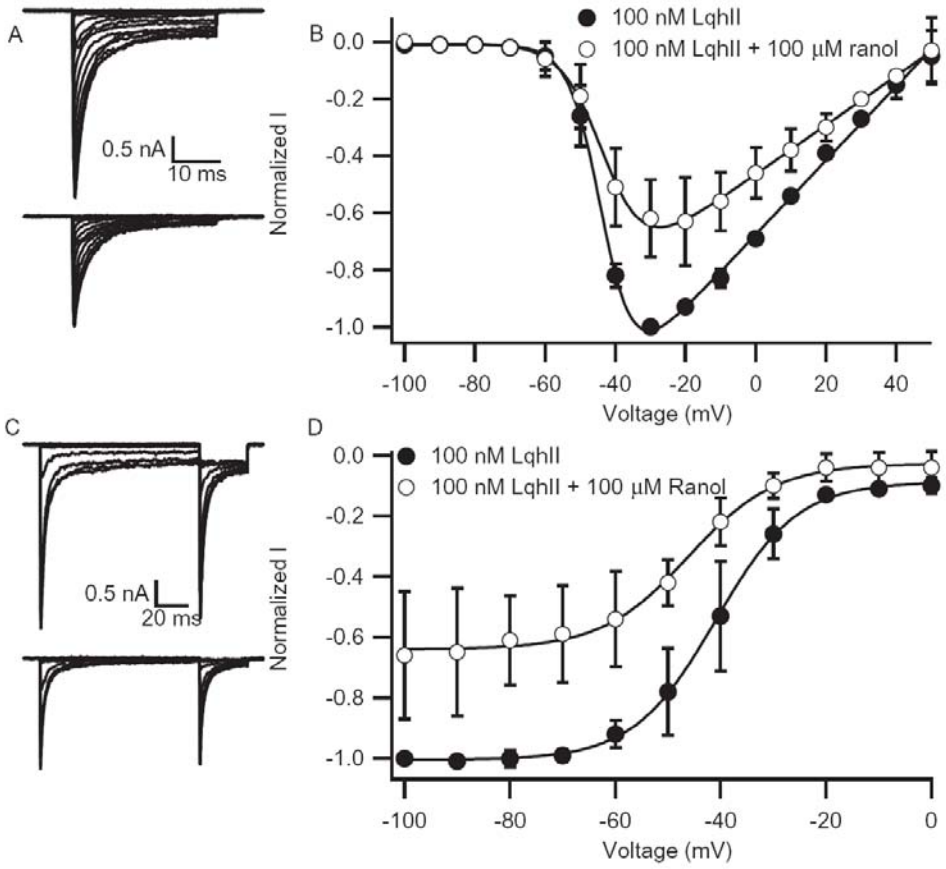
A
0.5 nA
10 ms
B
100 nM LqhII
100 nM LqhII + 100 µM ranol
Normalized I
0.0
-0.2
-0.4
-0.6
-0.8
-1.0
-100
-80
-60
-40
-20
0
20
40
Voltage (mV)
C
0.5 nA
20 ms
D
100 nM LqhII
100 nM LqhII + 100 µM Ranol
Normalized I
0.0
-0.2
-0.4
-0.6
-0.8
-1.0
-100
-80
-60
-40
-20
0
Voltage (mV)

Figure 19 Voltage-dependence of channel activation and fast inactivation before and after perfusion ranolazine.

(A) Representative current traces in the presence of 100 nM LqhII before (upper panel) and after perfusion (lower panel) of 100 μM ranolazine. The voltage-dependence of channel activation was measured from a holding potential of -100 mV depolarized to potentials from -100 mV to +50 mV in 10-mV increments. (B) Voltage-dependence of channel activation in the presence of 100 nM LqhII before and after perfusion 100 μM ranolazine. Currents from individual cells are normalized to the current measured at -30 mV before perfusion 100 μM ranolazine. $V_{0.5}$ (Before) = -43.4 ± 0.3 mV and $V_{0.5}$ (After) = -42.5 ± 0.4 mV, n = 3. (C) Representative current traces in the presence of 100 nM LqhII before (upper panel) and after perfusion (lower panel) of 100 μM ranolazine. The voltage-dependence of fast inactivation was measured from a holding potential of −100 mV. A test pulse to 0 mV was applied for 10 ms following a prepulse for 100 ms to potentials from −100 to 0 mV in 10-mV increments. (D) Voltage-dependence of channel fast inactivation in the presence of 100 nM LqhII before and after perfusion 100 μM ranolazine. Currents from individual cells are normalized to the current measured at -100 mV before perfusion 100 μM ranolazine. $V_{0.5}$ (Before) = -41.0 ± 0.3 mV and $V_{0.5}$ (After) = -46.1 ± 0.8 mV, n = 3.

References

(1) Catterall, W. A. (2000) From ionic currents to molecular mechanisms: the structure and function of voltage-gated sodium channels. *Neuron 26*, 13-25.

(2) Yu, F. H., and Catterall, W. A. (2004) The VGL-chanome: a protein superfamily specialized for electrical signaling and ionic homeostasis. *Sci STKE 2004*, re15.

(3) Catterall, W. A., Cestele, S., Yarov-Yarovoy, V., Yu, F. H., Konoki, K., and Scheuer, T. (2007) Voltage-gated ion channels and gating modifier toxins. *Toxicon 49*, 124-41.

(4) Cestele, S., and Catterall, W. A. (2000) Molecular mechanisms of neurotoxin action on voltage-gated sodium channels. *Biochimie 82*, 883-92.

(5) Chen, H., and Heinemann, S. H. (2001) Interaction of scorpion alpha-toxins with cardiac sodium channels: binding properties and enhancement of slow inactivation. *J Gen Physiol 117*, 505-18.

(6) Sheets, M. F., and Hanck, D. A. (1999) Gating of skeletal and cardiac muscle sodium channels in mammalian cells. *J Physiol 514 (Pt 2)*, 425-36.

(7) Campos, F. V., Chanda, B., Beirao, P. S., and Bezanilla, F. (2008) Alpha-scorpion toxin impairs a conformational change that leads to fast inactivation of muscle sodium channels. *J Gen Physiol 132*, 251-63.

(8) Rogers, J. C., Qu, Y., Tanada, T. N., Scheuer, T., and Catterall, W. A. (1996) Molecular determinants of high affinity binding of alpha-scorpion toxin and sea anemone toxin in the S3-S4 extracellular loop in domain IV of the Na+ channel alpha subunit. *J Biol Chem 271*, 15950-62.

(9) Catterall, W. A. (1986) Molecular properties of voltage-sensitive sodium channels. *Annu Rev Biochem 55*, 953-85.

(10) Yu, F. H., Westenbroek, R. E., Silos-Santiago, I., McCormick, K. A., Lawson, D., Ge, P., Ferriera, H., Lilly, J., DiStefano, P. S., Catterall, W. A., Scheuer, T., and Curtis, R. (2003) Sodium channel beta4, a new disulfide-linked auxiliary subunit with similarity to beta2. *J Neurosci 23*, 7577-85.

(11) McCormick, K. A., Srinivasan, J., White, K., Scheuer, T., and Catterall, W. A. (1999) The extracellular domain of the beta1 subunit is both necessary and sufficient for beta1-like modulation of sodium channel gating. *J Biol Chem 274*, 32638-46.

(12) Isom, L. L., Scheuer, T., Brownstein, A. B., Ragsdale, D. S., Murphy, B. J., and Catterall, W. A. (1995) Functional co-expression of the beta 1 and type IIA alpha subunits of sodium channels in a mammalian cell line. *J Biol Chem 270*, 3306-12.

(13) Morgan, K., Stevens, E. B., Shah, B., Cox, P. J., Dixon, A. K., Lee, K., Pinnock, R. D., Hughes, J., Richardson, P. J., Mizuguchi, K., and Jackson, A. P. (2000) beta 3: an additional auxiliary subunit of the voltage-sensitive sodium channel that modulates channel gating with distinct kinetics. *Proc Natl Acad Sci U S A 97*, 2308-13.

(14) Isom, L. L., De Jongh, K. S., Patton, D. E., Reber, B. F., Offord, J., Charbonneau, H., Walsh, K., Goldin, A. L., and Catterall, W. A. (1992) Primary structure and functional expression of the beta 1 subunit of the rat brain sodium channel. *Science 256*, 839-42.

(15) Isom, L. L., Ragsdale, D. S., De Jongh, K. S., Westenbroek, R. E., Reber, B. F., Scheuer, T., and Catterall, W. A. (1995) Structure and function of the beta 2 subunit of brain sodium channels, a transmembrane glycoprotein with a CAM motif. *Cell 83*, 433-42.

(16) Goldin, A. L., Barchi, R. L., Caldwell, J. H., Hofmann, F., Howe, J. R., Hunter, J. C., Kallen, R. G., Mandel, G., Meisler, M. H., Netter, Y. B., Noda, M., Tamkun, M. M., Waxman, S. G.,

Wood, J. N., and Catterall, W. A. (2000) Nomenclature of voltage-gated sodium channels. *Neuron 28*, 365-8.

(17) Hodgkin, A. L., and Huxley, A. F. (1952) A quantitative description of membrane current and its application to conduction and excitation in nerve. *J Physiol 117*, 500-44.

(18) Armstrong, C. M. (1981) Sodium channels and gating currents. *Physiol Rev 61*, 644-83.

(19) Catterall, W. A., and Yarov-Yarovoy, V. Helical motion of an S4 voltage sensor revealed by gating pore currents. *Channels (Austin) 4*, 75-7.

(20) Decaen, P. G., Yarov-Yarovoy, V., Scheuer, T., and Catterall, W. A. Gating charge interactions with the S1 segment during activation of a Na+ channel voltage sensor. *Proc Natl Acad Sci U S A 108*, 18825-30.

(21) DeCaen, P. G., Yarov-Yarovoy, V., Sharp, E. M., Scheuer, T., and Catterall, W. A. (2009) Sequential formation of ion pairs during activation of a sodium channel voltage sensor. *Proc Natl Acad Sci U S A 106*, 22498-503.

(22) DeCaen, P. G., Yarov-Yarovoy, V., Zhao, Y., Scheuer, T., and Catterall, W. A. (2008) Disulfide locking a sodium channel voltage sensor reveals ion pair formation during activation. *Proc Natl Acad Sci U S A 105*, 15142-7.

(23) Yarov-Yarovoy, V., Decaen, P. G., Westenbroek, R. E., Pan, C. Y., Scheuer, T., Baker, D., and Catterall, W. A. Structural basis for gating charge movement in the voltage sensor of a sodium channel. *Proc Natl Acad Sci U S A*.

(24) Booker, P. D., Whyte, S. D., and Ladusans, E. J. (2003) Long QT syndrome and anaesthesia. *Br J Anaesth 90*, 349-66.

(25) Stuhmer, W., Conti, F., Suzuki, H., Wang, X. D., Noda, M., Yahagi, N., Kubo, H., and Numa, S. (1989) Structural parts involved in activation and inactivation of the sodium channel. *Nature 339*, 597-603.

(26) West, J. W., Patton, D. E., Scheuer, T., Wang, Y., Goldin, A. L., and Catterall, W. A. (1992) A cluster of hydrophobic amino acid residues required for fast Na(+)-channel inactivation. *Proc Natl Acad Sci U S A 89*, 10910-4.

(27) Eaholtz, G., Scheuer, T., and Catterall, W. A. (1994) Restoration of inactivation and block of open sodium channels by an inactivation gate peptide. *Neuron 12*, 1041-8.

(28) McPhee, J. C., Ragsdale, D. S., Scheuer, T., and Catterall, W. A. (1995) A critical role for transmembrane segment IVS6 of the sodium channel alpha subunit in fast inactivation. *J Biol Chem 270*, 12025-34.

(29) Smith, M. R., and Goldin, A. L. (1997) Interaction between the sodium channel inactivation linker and domain III S4-S5. *Biophys J 73*, 1885-95.

(30) Filatov, G. N., Nguyen, T. P., Kraner, S. D., and Barchi, R. L. (1998) Inactivation and secondary structure in the D4/S4-5 region of the SkM1 sodium channel. *J Gen Physiol 111*, 703-15.

(31) McPhee, J. C., Ragsdale, D. S., Scheuer, T., and Catterall, W. A. (1998) A critical role for the S4-S5 intracellular loop in domain IV of the sodium channel alpha-subunit in fast inactivation. *J Biol Chem 273*, 1121-9.

(32) Tan, H. L., Bezzina, C. R., Smits, J. P., Verkerk, A. O., and Wilde, A. A. (2003) Genetic control of sodium channel function. *Cardiovasc Res 57*, 961-73.

(33) Lerche, H., Peter, W., Fleischhauer, R., Pika-Hartlaub, U., Malina, T., Mitrovic, N., and Lehmann-Horn, F. (1997) Role in fast inactivation of the IV/S4-S5 loop of the human muscle Na+ channel probed by cysteine mutagenesis. *J Physiol 505 (Pt 2)*, 345-52.

(34) Ptacek, L. J., George, A. L., Jr., Griggs, R. C., Tawil, R., Kallen, R. G., Barchi, R. L., Robertson, M., and Leppert, M. F. (1991) Identification of a mutation in the gene causing hyperkalemic periodic paralysis. *Cell 67*, 1021-7.

(35) Rojas, C. V., Wang, J. Z., Schwartz, L. S., Hoffman, E. P., Powell, B. R., and Brown, R. H., Jr. (1991) A Met-to-Val mutation in the skeletal muscle Na+ channel alpha-subunit in hyperkalaemic periodic paralysis. *Nature 354*, 387-9.

(36) McClatchey, A. I., Van den Bergh, P., Pericak-Vance, M. A., Raskind, W., Verellen, C., McKenna-Yasek, D., Rao, K., Haines, J. L., Bird, T., Brown, R. H., Jr., and et al. (1992) Temperature-sensitive mutations in the III-IV cytoplasmic loop region of the skeletal muscle sodium channel gene in paramyotonia congenita. *Cell 68*, 769-74.

(37) Ptacek, L. J., George, A. L., Jr., Barchi, R. L., Griggs, R. C., Riggs, J. E., Robertson, M., and Leppert, M. F. (1992) Mutations in an S4 segment of the adult skeletal muscle sodium channel cause paramyotonia congenita. *Neuron 8*, 891-7.

(38) Bennett, P. B., Yazawa, K., Makita, N., and George, A. L., Jr. (1995) Molecular mechanism for an inherited cardiac arrhythmia. *Nature 376*, 683-5.

(39) Wang, Q., Shen, J., Splawski, I., Atkinson, D., Li, Z., Robinson, J. L., Moss, A. J., Towbin, J. A., and Keating, M. T. (1995) SCN5A mutations associated with an inherited cardiac arrhythmia, long QT syndrome. *Cell 80*, 805-11.

(40) Catterall, W. A. (1980) Neurotoxins that act on voltage-sensitive sodium channels in excitable membranes. *Annu Rev Pharmacol Toxicol 20*, 15-43.

(41) Noda, M., Suzuki, H., Numa, S., and Stuhmer, W. (1989) A single point mutation confers tetrodotoxin and saxitoxin insensitivity on the sodium channel II. *FEBS Lett 259*, 213-6.

(42) Terlau, H., Heinemann, S. H., Stuhmer, W., Pusch, M., Conti, F., Imoto, K., and Numa, S. (1991) Mapping the site of block by tetrodotoxin and saxitoxin of sodium channel II. *FEBS Lett 293*, 93-6.

(43) Dudley, S. C., Jr., Todt, H., Lipkind, G., and Fozzard, H. A. (1995) A mu-conotoxin-insensitive Na+ channel mutant: possible localization of a binding site at the outer vestibule. *Biophys J 69*, 1657-65.

(44) Catterall, W. A. (1977) Activation of the action potential Na+ ionophore by neurotoxins. An allosteric model. *J Biol Chem 252*, 8669-76.

(45) Pauron, D., Barhanin, J., and Lazdunski, M. (1985) The voltage-dependent Na+ channel of insect nervous system identified by receptor sites for tetrodotoxin, and scorpion and sea anemone toxins. *Biochem Biophys Res Commun 131*, 1226-33.

(46) Schweitz, H., Vincent, J. P., Barhanin, J., Frelin, C., Linden, G., Hugues, M., and Lazdunski, M. (1981) Purification and pharmacological properties of eight sea anemone toxins from Anemonia sulcata, Anthopleura xanthogrammica, Stoichactis giganteus, and Actinodendron plumosum. *Biochemistry 20*, 5245-52.

(47) Nicholson, G. M., Walsh, R., Little, M. J., and Tyler, M. I. (1998) Characterisation of the effects of robustoxin, the lethal neurotoxin from the Sydney funnel-web spider Atrax robustus, on sodium channel activation and inactivation. *Pflugers Arch 436*, 117-26.

(48) Cahalan, M. D. (1975) Modification of sodium channel gating in frog myelinated nerve fibres by Centruroides sculpturatus scorpion venom. *J Physiol 244*, 511-34.

(49) Jover, E., Couraud, F., and Rochat, H. (1980) Two types of scorpion neurotoxins characterized by their binding to two separate receptor sites on rat brain synaptosomes. *Biochem Biophys Res Commun 95*, 1607-14.

(50) Jaimovich, E., Ildefonse, M., Barhanin, J., Rougier, O., and Lazdunski, M. (1982) Centruroides toxin, a selective blocker of surface Na+ channels in skeletal muscle:

voltage-clamp analysis and biochemical characterization of the receptor. *Proc Natl Acad Sci U S A 79*, 3896-900.

(51) Rochat, H., Bernard, P., and Couraud, F. (1979) Scorpion toxins: chemistry and mode of action. *Adv Cytopharmacol 3*, 325-34.

(52) Cestele, S., Qu, Y., Rogers, J. C., Rochat, H., Scheuer, T., and Catterall, W. A. (1998) Voltage sensor-trapping: enhanced activation of sodium channels by beta-scorpion toxin bound to the S3-S4 loop in domain II. *Neuron 21*, 919-31.

(53) Catterall, W. A., and Risk, M. (1981) Toxin T4(6) from Ptychodiscus brevis (formerly Gymnodinium breve) enhances activation of voltage-sensitive sodium channels by veratridine. *Mol Pharmacol 19*, 345-8.

(54) Trainer, V. L., Baden, D. G., and Catterall, W. A. (1994) Identification of peptide components of the brevetoxin receptor site of rat brain sodium channels. *J Biol Chem 269*, 19904-9.

(55) Trainer, V. L., Thomsen, W. J., Catterall, W. A., and Baden, D. G. (1991) Photoaffinity labeling of the brevetoxin receptor on sodium channels in rat brain synaptosomes. *Mol Pharmacol 40*, 988-94.

(56) Fainzilber, M., Kofman, O., Zlotkin, E., and Gordon, D. (1994) A new neurotoxin receptor site on sodium channels is identified by a conotoxin that affects sodium channel inactivation in molluscs and acts as an antagonist in rat brain. *J Biol Chem 269*, 2574-80.

(57) Kopeyan, C., Martinez, G., Lissitzky, S., Miranda, F., and Rochat, H. (1974) Disulfide bonds of toxin II of the scorpion Androctonus australis Hector. *Eur J Biochem 47*, 483-9.

(58) Gordon, D., and Gurevitz, M. (2003) The selectivity of scorpion alpha-toxins for sodium channel subtypes is determined by subtle variations at the interacting surface. *Toxicon 41*, 125-8.

(59) Gordon, D., Karbat, I., Ilan, N., Cohen, L., Kahn, R., Gilles, N., Dong, K., Stuhmer, W., Tytgat, J., and Gurevitz, M. (2007) The differential preference of scorpion alpha-toxins for insect or mammalian sodium channels: implications for improved insect control. *Toxicon 49*, 452-72.

(60) Housset, D., Habersetzer-Rochat, C., Astier, J. P., and Fontecilla-Camps, J. C. (1994) Crystal structure of toxin II from the scorpion Androctonus australis Hector refined at 1.3 A resolution. *J Mol Biol 238*, 88-103.

(61) Fontecilla-Camps, J. C., Habersetzer-Rochat, C., and Rochat, H. (1988) Orthorhombic crystals and three-dimensional structure of the potent toxin II from the scorpion Androctonus australis Hector. *Proc Natl Acad Sci U S A 85*, 7443-7.

(62) Kahn, R., Karbat, I., Ilan, N., Cohen, L., Sokolov, S., Catterall, W. A., Gordon, D., and Gurevitz, M. (2009) Molecular requirements for recognition of brain voltage-gated sodium channels by scorpion alpha-toxins. *J Biol Chem 284*, 20684-91.

(63) Karbat, I., Frolow, F., Froy, O., Gilles, N., Cohen, L., Turkov, M., Gordon, D., and Gurevitz, M. (2004) Molecular basis of the high insecticidal potency of scorpion alpha-toxins. *J Biol Chem 279*, 31679-86.

(64) Guan, R. J., Xiang, Y., He, X. L., Wang, C. G., Wang, M., Zhang, Y., Sundberg, E. J., and Wang, D. C. (2004) Structural mechanism governing cis and trans isomeric states and an intramolecular switch for cis/trans isomerization of a non-proline peptide bond observed in crystal structures of scorpion toxins. *J Mol Biol 341*, 1189-204.

(65) Turkov, M., Rashi, S., Noam, Z., Gordon, D., Ben Khalifa, R., Stankiewicz, M., Pelhate, M., and Gurevitz, M. (1997) In vitro folding and functional analysis of an anti-insect selective

scorpion depressant neurotoxin produced in Escherichia coli. *Protein Expr Purif 10*, 123-31.

(66) Bosmans, F., Martin-Eauclaire, M. F., and Swartz, K. J. (2008) Deconstructing voltage sensor function and pharmacology in sodium channels. *Nature 456*, 202-8.

(67) Vassilev, P. M., Scheuer, T., and Catterall, W. A. (1988) Identification of an intracellular peptide segment involved in sodium channel inactivation. *Science 241*, 1658-61.

(68) Tejedor, F. J., and Catterall, W. A. (1988) Site of covalent attachment of alpha-scorpion toxin derivatives in domain I of the sodium channel alpha subunit. *Proc Natl Acad Sci U S A 85*, 8742-6.

(69) Thomsen, W. J., and Catterall, W. A. (1989) Localization of the receptor site for alpha-scorpion toxins by antibody mapping: implications for sodium channel topology. *Proc Natl Acad Sci U S A 86*, 10161-5.

(70) Li-Smerin, Y., and Swartz, K. J. (1998) Gating modifier toxins reveal a conserved structural motif in voltage-gated Ca2+ and K+ channels. *Proc Natl Acad Sci U S A 95*, 8585-9.

(71) Li-Smerin, Y., and Swartz, K. J. (2000) Localization and molecular determinants of the Hanatoxin receptors on the voltage-sensing domains of a K(+) channel. *J Gen Physiol 115*, 673-84.

(72) Bourinet, E., Soong, T. W., Sutton, K., Slaymaker, S., Mathews, E., Monteil, A., Zamponi, G. W., Nargeot, J., and Snutch, T. P. (1999) Splicing of α_{1A} subunit gene generates phenotypic variants of P- and Q-type calcium channels. *Nat Neurosci 2*, 407-15.

(73) Winterfield, J. R., and Swartz, K. J. (2000) A hot spot for the interaction of gating modifier toxins with voltage-dependent ion channels. *J Gen Physiol 116*, 637-44.

(74) Catterall, W. A. (1977) Membrane potential-dependent binding of scorpion toxin to the action potential Na+ ionophore. Studies with a toxin derivative prepared by lactoperoxidase-catalyzed iodination. *J Biol Chem 252*, 8660-8.

(75) Yarov-Yarovoy, V., Baker, D., and Catterall, W. A. (2006) Voltage sensor conformations in the open and closed states in ROSETTA structural models of K^+ channels. *Proc Natl Acad Sci U S A 103*, 7292-7.

(76) Yarov-Yarovoy, V., Schonbrun, J., and Baker, D. (2006) Multipass membrane protein structure prediction using Rosetta. *Proteins 62*, 1010-25.

(77) Jeanmougin, F., Thompson, J. D., Gouy, M., Higgins, D. G., and Gibson, T. J. (1998) Multiple sequence alignment with Clustal X. *Trends Biochem Sci 23*, 403-5.

(78) Yarov-Yarovoy, V., DeCaen, P. G., Westenbroek, R. E., Pan, C. Y., Scheuer, T., Baker, D., and Catterall, W. A. Structural basis for gating charge movement in the voltage sensor of a sodium channel. *Proc Natl Acad Sci U S A 109*, E93-102.

(79) Rohl, C. A., Strauss, C. E., Misura, K. M., and Baker, D. (2004) Protein structure prediction using Rosetta. *Methods Enzymol 383*, 66-93.

(80) Gray, J. J., Moughon, S., Wang, C., Schueler-Furman, O., Kuhlman, B., Rohl, C. A., and Baker, D. (2003) Protein-protein docking with simultaneous optimization of rigid-body displacement and side-chain conformations. *J Mol Biol 331*, 281-99.

(81) Wang, C., Bradley, P., and Baker, D. (2007) Protein-protein docking with backbone flexibility. *J Mol Biol 373*, 503-19.

(82) Chen, H., Lu, S., Leipold, E., Gordon, D., Hansel, A., and Heinemann, S. H. (2002) Differential sensitivity of sodium channels from the central and peripheral nervous system to the scorpion toxins Lqh-2 and Lqh-3. *Eur J Neurosci 16*, 767-70.

(83) Leipold, E., Lu, S., Gordon, D., Hansel, A., and Heinemann, S. H. (2004) Combinatorial interaction of scorpion toxins Lqh-2, Lqh-3, and LqhalphaIT with sodium channel receptor sites-3. *Mol Pharmacol 65*, 685-91.

(84) Long, S. B., Tao, X., Campbell, E. B., and MacKinnon, R. (2007) Atomic structure of a voltage-dependent K+ channel in a lipid membrane-like environment. *Nature 450*, 376-82.

(85) Pathak, M. M., Yarov-Yarovoy, V., Agarwal, G., Roux, B., Barth, P., Kohout, S., Tombola, F., and Isacoff, E. Y. (2007) Closing in on the resting state of the Shaker K(+) channel. *Neuron 56*, 124-40.

(86) Cestele, S., Yarov-Yarovoy, V., Qu, Y., Sampieri, F., Scheuer, T., and Catterall, W. A. (2006) Structure and function of the voltage sensor of sodium channels probed by a beta-scorpion toxin. *J Biol Chem 281*, 21332-44.

(87) Leipold, E., Hansel, A., Borges, A., and Heinemann, S. H. (2006) Subtype specificity of scorpion beta-toxin Tz1 interaction with voltage-gated sodium channels is determined by the pore loop of domain 3. *Mol Pharmacol 70*, 340-7.

(88) Catterall, W. A. (1979) Binding of scorpion toxin to receptor sites associated with sodium channels in frog muscle. Correlation of voltage-dependent binding with activation. *J Gen Physiol 74*, 375-91.

(89) Jiang, Y., Lee, A., Chen, J., Cadene, M., Chait, B. T., and MacKinnon, R. (2002) Crystal structure and mechanism of a calcium-gated potassium channel. *Nature 417*, 515-22.

(90) Long, S. B., Campbell, E. B., and Mackinnon, R. (2005) Crystal structure of a mammalian voltage-dependent Shaker family K^+ channel. *Science 309*, 897-903.

(91) Long, S. B., Campbell, E. B., and Mackinnon, R. (2005) Voltage sensor of Kv1.2: structural basis of electromechanical coupling. *Science 309*, 903-8.

(92) Karbat, I., Kahn, R., Cohen, L., Ilan, N., Gilles, N., Corzo, G., Froy, O., Gur, M., Albrecht, G., Heinemann, S. H., Gordon, D., and Gurevitz, M. (2007) The unique pharmacology of the scorpion alpha-like toxin Lqh3 is associated with its flexible C-tail. *Febs J 274*, 1918-31.

(93) Zilberberg, N., Froy, O., Loret, E., Cestele, S., Arad, D., Gordon, D., and Gurevitz, M. (1997) Identification of structural elements of a scorpion alpha-neurotoxin important for receptor site recognition. *J Biol Chem 272*, 14810-6.

(94) Pettersen, E. F., Goddard, T. D., Huang, C. C., Couch, G. S., Greenblatt, D. M., Meng, E. C., and Ferrin, T. E. (2004) UCSF Chimera--a visualization system for exploratory research and analysis. *J Comput Chem 25*, 1605-12.

(95) Waterhouse, A. M., Procter, J. B., Martin, D. M., Clamp, M., and Barton, G. J. (2009) Jalview Version 2--a multiple sequence alignment editor and analysis workbench. *Bioinformatics 25*, 1189-91.

(96) Gur, M., Kahn, R., Karbat, I., Regev, N., Wang, J., Catterall, W. A., Gordon, D., and Gurevitz, M. Elucidation of the molecular basis of selective recognition uncovers the interaction site for the core domain of scorpion alpha-toxins on sodium channels. *J Biol Chem 286*, 35209-17.

(97) Wang, J., Yarov-Yarovoy, V., Kahn, R., Gordon, D., Gurevitz, M., Scheuer, T., and Catterall, W. A. Mapping the receptor site for alpha-scorpion toxins on a Na+ channel voltage sensor. *Proc Natl Acad Sci U S A 108*, 15426-31.

(98) Ranganathan, R., Lewis, J. H., and MacKinnon, R. (1996) Spatial localization of the K+ channel selectivity filter by mutant cycle-based structure analysis. *Neuron 16*, 131-9.

(99) Kash, T. L., Jenkins, A., Kelley, J. C., Trudell, J. R., and Harrison, N. L. (2003) Coupling of agonist binding to channel gating in the GABA(A) receptor. *Nature 421*, 272-5.

(100) Benzinger, G. R., Kyle, J. W., Blumenthal, K. M., and Hanck, D. A. (1998) A specific interaction between the cardiac sodium channel and site-3 toxin anthopleurin B. *J Biol Chem 273*, 80-4.
(101) Carter, P. J., Winter, G., Wilkinson, A. J., and Fersht, A. R. (1984) The use of double mutants to detect structural changes in the active site of the tyrosyl-tRNA synthetase (Bacillus stearothermophilus). *Cell 38*, 835-40.
(102) Burley, S. K., and Petsko, G. A. (1985) Aromatic-aromatic interaction: a mechanism of protein structure stabilization. *Science 229*, 23-8.
(103) Fredj, S., Sampson, K. J., Liu, H., and Kass, R. S. (2006) Molecular basis of ranolazine block of LQT-3 mutant sodium channels: evidence for site of action. *Br J Pharmacol 148*, 16-24.
(104) El-Bizri, N., Kahlig, K. M., Shyrock, J. C., George, A. L., Jr., Belardinelli, L., and Rajamani, S. Ranolazine block of human Na v 1.4 sodium channels and paramyotonia congenita mutants. *Channels (Austin) 5*, 161-72.
(105) Wang, G. K., Calderon, J., and Wang, S. Y. (2008) State- and use-dependent block of muscle Nav1.4 and neuronal Nav1.7 voltage-gated Na+ channel isoforms by ranolazine. *Mol Pharmacol 73*, 940-8.
(106) Song, Y., Shryock, J. C., Wu, L., and Belardinelli, L. (2004) Antagonism by ranolazine of the pro-arrhythmic effects of increasing late INa in guinea pig ventricular myocytes. *J Cardiovasc Pharmacol 44*, 192-9.
(107) West, J. W., Scheuer, T., Maechler, L., and Catterall, W. A. (1992) Efficient expression of rat brain type IIA Na+ channel alpha subunits in a somatic cell line. *Neuron 8*, 59-70.